Journal of Medicinal Chemistry

Article

pubs.acs.org/jmc

Optimized Protein Kinase Cθ (PKCθ) Inhibitors Reveal Only Modest Anti-inflammatory Efficacy in a Rodent Model of Arthritis

Dawn M. George,*[,†] Eric C. Breinlinger,[†] Maria A. Argiriadi,[†] Yang Zhang,[∥] Jianfei Wang,[∥] Pratima Bansal-Pakala,[†] David B. Duignan,[†] Prisca Honore,[‡] QingYu Lang,[§] Scott Mittelstadt,[‡] Lian Rundell,[†] Annette Schwartz,[†] Jiakang Sun,[∥] and Jeremy J. Edmunds[†]

[†]AbbVie Bioresearch Center, 381 Plantation Street, Worcester, Massachusetts 01605, United States

[‡]AbbVie, Inc., 1 North Waukegan Road, North Chicago, Illinois 60064, United States

[§]AbbVie China R&D Center, 5F, North Jin Chuang Building #1, 4560 Jinke Road, Pudong New District, Shanghai 201201, P. R. China

[∥]WuXi AppTec (Shanghai) Co., Ltd., 288 Fute Zhong Road, Waigaoqiao Free Trade Zone, Shanghai 200131, P. R. China

Supporting Information

ABSTRACT: We previously demonstrated that selective inhibition of protein kinase Cθ (PKCθ) with triazinone **1** resulted in dose-dependent reduction of paw swelling in a mouse model of arthritis.[1,2] However, a high concentration was required for efficacy, thus providing only a minimal safety window. Herein we describe a strategy to deliver safer compounds based on the hypothesis that optimization of potency in concert with good oral pharmacokinetic (PK) properties would enable in vivo efficacy at reduced exposures, resulting in an improved safety window. Ultimately, transformation of **1** yielded analogues that demonstrated excellent potency and PK properties and fully inhibited IL-2 production in an acute model. In spite of good exposure, twice-a-day treatment with **17l** in the glucose-6-phosphate isomerase chronic in vivo mouse model of arthritis yielded only moderate efficacy. On the basis of the exposure achieved, we conclude that PKCθ inhibition alone is insufficient for complete efficacy in this rodent arthritis model.

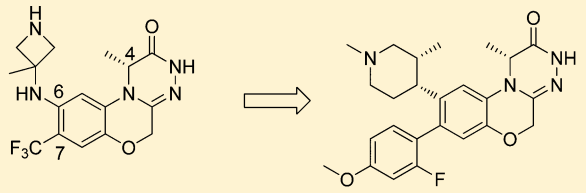

INTRODUCTION

Inhibition of protein kinase Cθ (PKCθ) blocks the activation of T cells[3−5] and thus is hypothesized to ameliorate T-cell-mediated disease states such as rheumatoid arthritis (RA), inflammatory bowel disease (IBD), and psoriasis. Multiple companies have worked to identify suitable chemical matter to inhibit this intriguing target that is predominately expressed in T cells.[6−17] In our previous paper, we detailed the discovery of potent and selective PKCθ inhibitor triazinone **1**.[1] Compound **1** has moderate cellular potency (IC_{50} = 0.12 μM) and permeability (Papp A to B = 2.1 × 10^{-6} cm/s), good oral pharmacokinetics (PK) in mouse (CL = 1.5 L h^{-1} kg^{-1}, $t_{1/2}$ = 3.1 h; F = 108%), and efficacy in acute [concanavalin A (Con A)-induced IL-2 production, ED_{80} = 29 mg/kg] and chronic [glucose-6-phosphate isomerase (GPI)-induced arthritis,[18,19] 61% inhibition of paw swelling at 10 mg/kg and 100% inhibition of paw swelling at 30 mg/kg when dosed in a full prophylactic mode] in vivo mouse models. Although a retrospective analysis of the utility of preclinical arthritis models [rat adjuvant-induced arthritis (AIA), rat collagen-induced arthritis (CIA), and mouse CIA] concluded that efficacy with therapeutic treatment is more likely to predict efficacy in human RA patients,[20] the predictive value of the GPI model, whether utilizing therapeutic or prophylactic dosing, remains to be determined. In our studies with **1**, high efficacious exposure and full coverage over the unbound cellular EC_{80} were essential to drive efficacy in the chronic study, and serious tolerability issues were encountered after ∼10 days of oral administration at doses only 3-fold higher than that required for efficacy. Unable to identify a specific off-target protein to which the toxicities could be attributed, we turned our focus toward identifying compounds with reduced efficacious exposures as an approach to potentially amplify the therapeutic index. In this paper, we describe structure-based optimization starting from compound **1** that led to the discovery of compounds with improved cellular potency coupled with desirable PK profiles. Progression of promising compounds into a screening version of the acute in vivo Con A model in mice enabled rapid selection of compounds for advancement into the chronic in vivo GPI mouse model of arthritis to test their efficacy and tolerability.

Special Issue: New Frontiers in Kinases

Received: August 26, 2014
Published: September 25, 2014

Scheme 1[a]

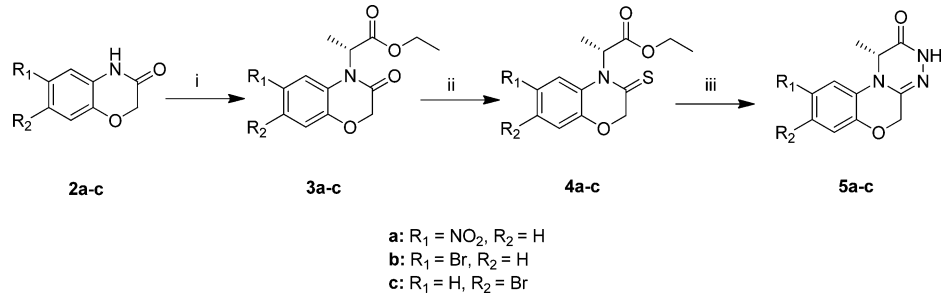

[a]Reagents and conditions: (i) KHMDS, (*S*)-2-trifluoromethanesulfonyloxypropionic acid ethyl ester, THF, 0 °C to rt; (ii) Lawesson reagent, toluene, 120 °C; (iii) $NH_2NH_2{\cdot}H_2O$, EtOH, rt.

Scheme 2[a]

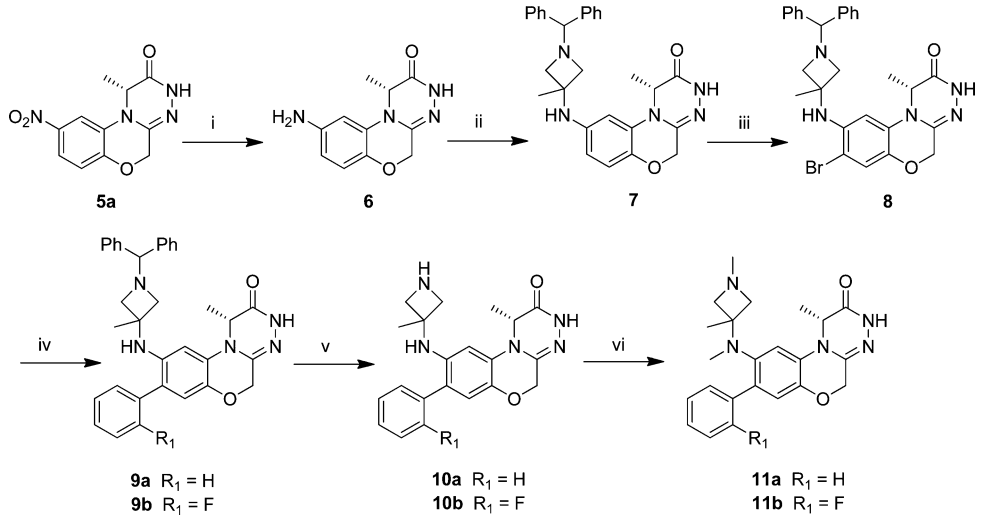

[a]Reagents and conditions: (i) NH_4Cl, Zn powder, MeOH, THF, 50 °C; (ii) 1-benzhydryl-3-methylazetidin-3-yl methanesulfonate, K_2CO_3, propan-2-ol, 80 °C; (iii) nBu_4NBr_3, DCM, MeOH, rt; (iv) R_1-phenylboronic acid or boronate ester, K_2CO_3, $Pd(dppf)_2Cl_2$, water, 1,4-dioxane, 80 °C; (v) $Pd(OH)_2/C$, HCl, MeOH, THF, H_2 (55 psi), 50 °C; (vi) paraformaldehyde, MeOH, AcOH, reflux, then $NaBH_3CN$, rt.

CHEMISTRY

The synthesis of triazinone **1**, prepared as a racemic mixture followed by late-stage chiral separation, was described previously.[1,2] An improved synthesis was developed to construct multifunctional triazinone intermediates **5a–c** with the *R* stereochemistry set at the 4-position (Scheme 1), eliminating the need for a chiral separation step. Alkylation of functionalized benzo[1,4]oxazinones **2a–c** with (*S*)-2-trifluoromethanesulfonyloxypropionic acid ethyl ester [generated by treatment of (*S*)-ethyl lactate with triflic anhydride] gave **3a–c**. Conversion to benzo[1,4]oxazinethiones **4a–c** by treatment with Lawesson reagent and subsequent cyclization with hydrazine hydrate afforded versatile triazinone intermediates **5a–c**. Bromide **5b** could be further transformed to the boronate ester (R_1 = pinacolatoboron, R_2 = H, **5d**) by treatment with bispinacolato(diboron). Elaboration of the triazinone core to access 6-aminoazetidine-substituted analogues proceeded as described in Scheme 2. Starting from 6-nitro intermediate **5a**, zinc-mediated reduction provided aniline **6**, and reaction with a 3-methylazetidine methanesulfonate yielded aminoazetidine **7**. Conversion to bromide **8** followed by Suzuki coupling with phenylboronic acids gave access to compounds **9a** and **9b**. Palladium-catalyzed hydrogenation yielded unmasked azetidines **10a** and **10b**, which were methylated by reductive amination to give analogues **11a** and **11b**.

A representative synthetic route to 6-piperidine-substituted triazinones **17a–l** is detailed in Scheme 3. From chiral 6-bromide **5d**, Suzuki cross-coupling with a tetrahydropyridin-4-yl triflate and chiral separation gave **12**. Subsequent hydrogenation provided piperidine **13** stereoselectively. Treatment with tetrabutylammonium bromide yielded bromide **14**, which underwent acid-mediated Boc deprotection to provide piperidine **15**. A penultimate methylation step yielded *N*-methylpiperidine **16**, and final Suzuki coupling afforded 7-aryl substituted analogues **17a–l**. Alternatively, the order of functionalization steps may be reversed. Thus, Suzuki coupling with bromide **14** followed by piperidine Boc deprotection and methylation also allows access to **17**.

7-Methyl-substituted analogue **18** (Figure 1) was prepared as previously described.[1,2] Methylated 6-aminoazetidine analogues **19–21** were prepared from **1** by sequential reductive amination reactions (see the Supporting Information). Similarly, 7-Ph-substituted analogue **22** was prepared by reductive amination of azetidine **10a**.

Preparation of 6-CH_2-azetidine analogue **23** was accomplished by Suzuki coupling with 6-boronate ester **5d**, reduction, and further functionalization as detailed in the Supporting

dx.doi.org/10.1021/jm5013006 | J. Med. Chem. 2015, 58, 333–346

Scheme 3[a]

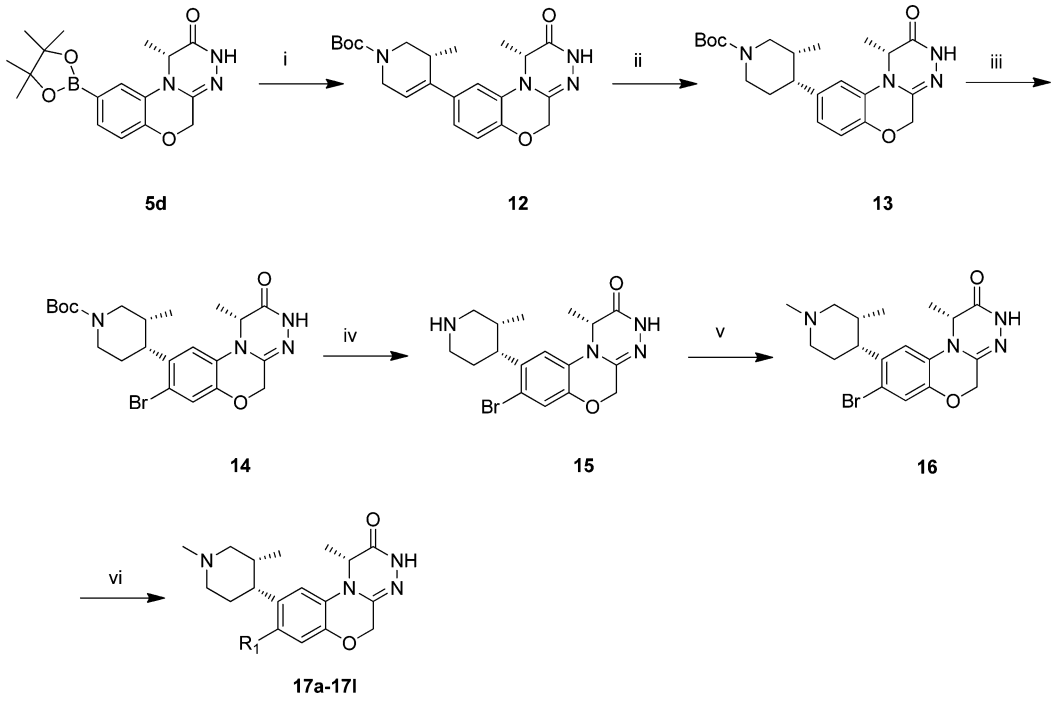

[a]Reagents and conditions: (i) 3-methyl-4-trifluoromethansulfonyloxy-3,6-dihydro-2*H*-pyridine-1-carboxylic acid *tert*-butyl ester, K_3PO_4, $Pd(Ph_3P)_4$, DMF, water, 80 °C, then chiral separation; (ii) Pd/C, H_2 (1 atm), MeOH, rt; (iii) nBu_4NBr_3, DCM, MeOH, rt; (iv) HCl, EtOAc, rt; (v) paraformaldehyde, $NaBH_3CN$, MeOH, AcOH, rt; (vi) R_1-boronic acid or boronate ester, K_2CO_3, $PdCl_2(dppf)-CH_2Cl_2$, 1,4-dioxane, water, 90 °C.

Information. 6-Piperidine and 6-pyrrolidine analogues **24**–**26** were prepared from 7-bromide **5c** via sequential Suzuki coupling, bromination at the 6-position, a second Suzuki coupling with the corresponding 5,6-dihydropyridine boronate ester or 2,5-dihydropyrrole boronate ester, and reduction steps (see the Supporting Information). Analogues **27**–**30** were prepared using methods similar to those described above (see the Supporting Information for details).

RESULTS AND DISCUSSION

Our previously reported PKCθ cocrystal structure with compound **18** (2.6 Å, PDB accession code 4Q9Z)[1] a structural relative of analogue **1**, confirmed the binding mode of the triazinone core (Figure 1). The N–N–H of the triazinone ring makes a hinge interaction with backbone residues Glu459 and Leu461, the C═O makes a water-mediated interaction with Thr442 in the back pocket, and the azetidine NH tightly contacts Asp522 and Asn509. Our initial design strategy was to introduce small groups around the aminoazetidine fragment, targeting occupation of lipophilic regions of the protein active site to enhance potency while maintaining or improving on the favorable PK profile observed with parent compound **1**. Methylation at either the anilino or azetidinyl nitrogen (**19** or **20**, respectively; Table 1) in the context of the 7-CF_3 moiety provided no improvement in potency. Notably, terminal methylation to give tertiary amine **20** did significantly improve the permeability (Papp A to B = 19 × 10^{-6} cm/s). Polymethylation, as in **21**, resulted in a significant deterioration in potency that could be explained by a potentially inefficient ligand conformation that is unable to reach target residues Asp522, Asn509, or Asp508. On the basis of our previous work, we predicted that a 7-Ph moiety would improve potency but could suffer from suboptimal PK. Accordingly, in the context of the 7-Ph group, the introduction of a methyl group on the azetidine nitrogen (**22**) was tolerated, similar to the activity

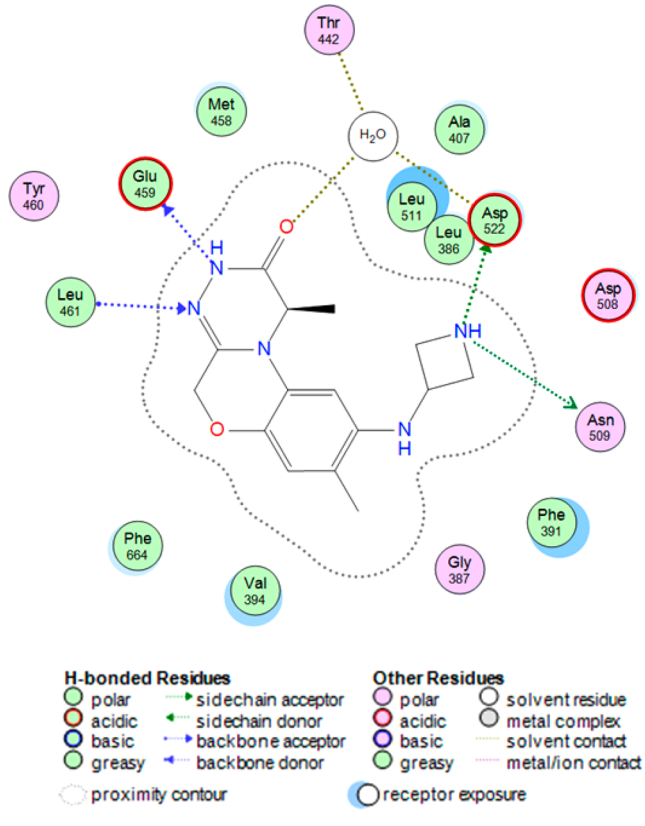

Figure 1. Key binding interactions of compound **18**, generated using the ligand interaction tool in MOE.[21]

dx.doi.org/10.1021/jm5013006 | *J. Med. Chem.* 2015, 58, 333–346

Table 1. Structure–Activity Relationships for Conformationally Constrained Variants[a]

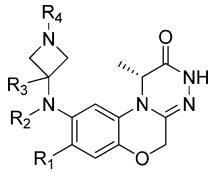

compd	R_1	R_2	R_3	R_4	PKCθ IC_{50} (μM)[a]	IL-2 IC_{50} (μM)[a]	permeability (10^{-6} cm/s)[b]	hu/mu $CL_{int,u}$ (L h^{-1} kg^{-1})[c]
1	CF_3	H	Me	H	0.023	0.12	2.1	<2.0/<5.7
19	CF_3	Me	Me	H	0.059	0.49	–	6.4/46
20	CF_3	H	Me	Me	0.057	0.37	19	–/–
21	CF_3	Me	Me	Me	0.70	3.0	–	6.0/39
22	Ph	H	Me	Me	0.052	0.23	24	5.0/17
11a	Ph	Me	Me	Me	0.004	0.037	15	15/68
11b	2-F-Ph	Me	Me	Me	0.004	0.024	15	18/134

[a]Means from $n \geq 2$ experiments. [b]MDCK-MDR1 with 40 μM CSA (pH 7.4) Papp A to B. [c]In vivo predicted unbound CL_{int} from human and mouse microsome stability studies.

pattern observed with related 7-CF_3-substituted triazinone **20**. Incorporation of an additional methyl group on the anilino-N linker (**11a**) provided a significant improvement in cellular activity, in stark contrast to 7-CF_3-substituted analogue **21**. Ligand minimization calculations and torsion analysis with **11a** suggested that the combination of two neighboring methyl groups on the aminoazetidine fragment and the presence of the 7-phenyl group result in an energetically favored minimum. The resulting ligand conformation provides preferential access to a different azetidine trajectory than observed with previous analogues. On the basis of this hypothesis, the azetidine nitrogen of **11a** would be positioned with the basic amine flipped "up" to target Asp508, whereas the azetidine nitrogen of compound **22** is oriented "down" to interact with Asp522 and Asn509 as seen with compound **18**. A crystal structure of **11a** in PKCθ (2.61 Å, PDB accession code 4RA5; Figure 2a) confirmed our hypothesis. The azetidine nitrogen has interactions with both the backbone carbonyl and side chain of Asp508. In comparison to our previously reported protein X-ray structure of triazinone **18** bound to PKCθ,[1] a protein backbone shift (~3.0 Å) is observed at the tip of the glycine-rich loop (Figure 2b), most likely because of 7-phenyl accommodation. Similar to observations from the previous structure, an ordered C-terminal extension proximal to residues Pro658–Leu669 is observed. A hydrophobic pocket formed as a result of this protein ordering provides an optimal fit for the 7-phenyl substituent. The pocket is surrounded by aromatic residues, including Phe391 (glycine-rich loop), Phe664 (C-terminal extension), and Phe668 (C-terminal extension).

In spite of the excellent in vitro potency of **11a**, in comparison to parent molecule **1** this compound suffered from higher microsomal clearance (mouse $CL_{int,u}$ = 68 L h^{-1} kg^{-1} compared with <5.7 L h^{-1} kg^{-1} for **1**) and high in vivo clearance (CL = 6.0 L h^{-1} kg^{-1} vs 1.5 L h^{-1} kg^{-1} for **1**) in mouse PK studies (Table 2). We suspected that demethylation of the azetidine *N*-Me was occurring, but metabolite identification (met ID) studies indicated that the major metabolite was formed by *aniline* demethylation of **11a**, which was a potential cause of the increased CL. Although the introduction of a 2-F group on the phenyl ring (**11b**) had a minimal impact on potency (cell IC_{50} = 0.024 μM for **11b** vs 0.037 μM for **11a**) and resulted in a moderately higher microsomal $CL_{int,u}$ (134 L h^{-1} kg^{-1} compared with 68 L h^{-1} kg^{-1} for **11a**), it did afford improved in vivo clearance (CL = 3.1 L h^{-1} kg^{-1}) and reasonable unbound oral exposure (AUC,u = 102 ng h mL^{-1}, 10 mg/kg dose). In contrast to **11a**, minimal aniline demethylation was observed in met ID studies in the case of **11b**, but significant demethylation of the azetidine *N*-Me occurred. In mouse PK with **11b**, exposure of the active

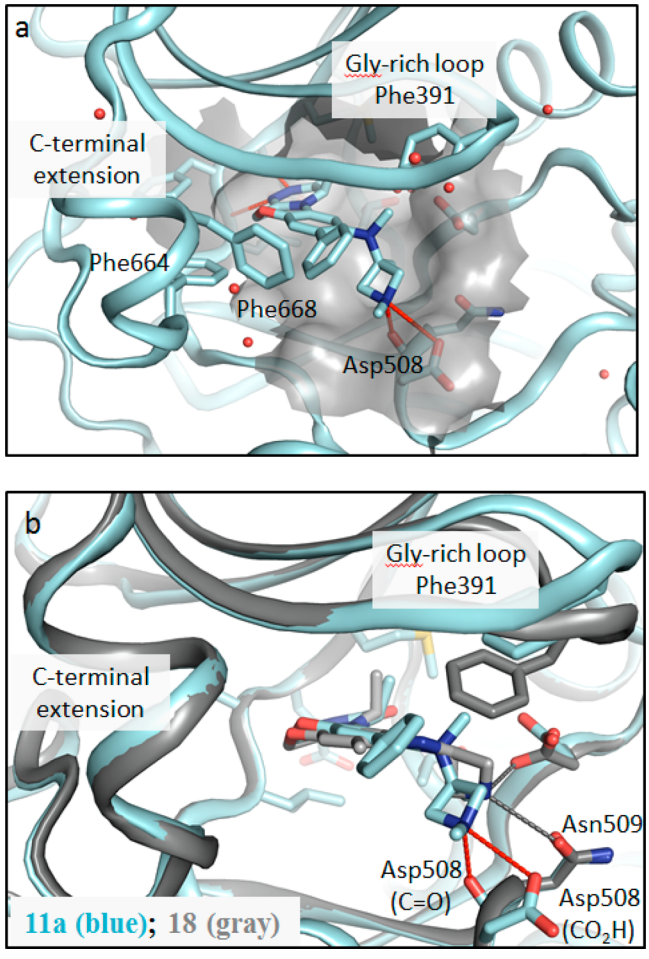

Figure 2. X-ray crystal structure of **11a** in PKCθ. Shown are (a) the X-ray crystal structure of **11a** (PDB accession code 4RA5) and (b) an overlay of the X-ray crystal structures of **11a** (blue) and **18** (gray) in PKCθ.

dx.doi.org/10.1021/jm5013006 | J. Med. Chem. 2015, 58, 333–346

Table 2. Comparison of Mouse PK for Compounds with 6-N versus 6-C Linkers

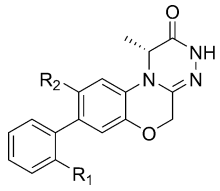

compd	11a	11b	23[e]	24[e]	25[e]	26
R_1	H	F	F	F	F	F
R_2	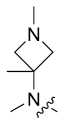	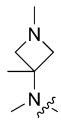	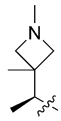			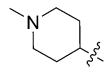
PKCθ IC_{50}[a] (μM)	0.004	0.004	0.003	0.042	0.041	0.043
IL-2 IC_{50}[a] (μM)	0.037	0.024	0.047	0.21	0.20	0.20
$CL_{int,u}$[b], hu/mu (L/h/kg)	15 / 68	18 / 134	16 / 214	6.2 / --	6.4 / 30	6.2 / 38
CL (L/h/kg)[c]	6.0	3.1	3.5	2.1[f]	4.2	1.5
CL,u (L/h/kg)[c]	71	33	22	19[f]	30	14
t1/2 (h)[c]	1.0	1.6	3.6	4.3[f]	7.5	5.1
Cmax,u (ng/mL)[c]	14.5	27.3	36.7	112[f]	39.9	67.0
AUC,u parent (ng*h/mL)[c]	37.3	102	132	920[f]	120	401
AUC,u metab. (ng*h/mL)[c,d]	NM[g]	83.2	NM[g]	111[f]	NM[g]	56.3
F (%)[c]	26	28	29	110[f]	33	54

[a]Means from $n \geq 2$ experiments. [b]In vivo predicted unbound CL_{int} from human and mouse microsome stability studies. [c]Mouse PK reported (3 mg/kg iv bolus in 50% PEG400; po dose of 10 mg/kg in 0.5% HPMC and 0.02% Tween80). Data are reported as averages of three animals. [d]AUC of desmethyl metabolite measured in the mouse PK study. [e]The absolute stereochemistry at the C6 linker was not determined. [f]The compound was not tolerated with a 3 mg/kg iv bolus; the value shown is from a 1 mg/kg iv bolus. [g]Not measured.

azetidine *N*-desmethyl metabolite (AUC,u = 83 ng h mL^{-1}, 10 mg/kg dose) was ~80% that of the parent (102 ng h mL^{-1}).

Because of the reasonable clearance observed with 7-(2-fluorophenyl)-substituted **11b**, we chose to incorporate this moiety in subsequent analogues while exploring alternative linkers at the 6-position. In order to prevent potential demethylation at the aniline position, the two isomeric analogues with a methylene linker (exemplified by compound **23**; Table 2) were prepared. Of the two isomers generated, one was >250-fold more potent than the other (PKCθ IC_{50} = 0.003 and 0.77 μM; the absolute stereochemistry was not determined). The linker change to CHMe from NMe was tolerated in terms of potency, but no improvement in in vivo clearance compared to **11b** (CL = 3.5 L h^{-1} kg^{-1} for **23**; CL = 3.1 L h^{-1} kg^{-1} for **11b**) or bioavailability (F = 29 and 28%, respectively) was observed. Considering the increasingly complex synthetic route and purification required to access analogues like **23** but encouraged by the promise of 6-C-linked analogues, we turned our attention to conformationally constrained pyrrolidine or piperidine moieties at the 6-position (**24**–**26**; Table 2). This approach initially yielded a moderate (~10-fold) reduction in potency, with all three analogues displaying nearly identical profiles in PKCθ enzyme (IC_{50} = 0.041–0.043 μM) and cellular (IC_{50} = 0.20–0.21 μM) assays and acceptable mouse microsomal clearance ($CL_{int,u}$ = 30–38 L h^{-1} kg^{-1}). Mouse PK studies revealed an interesting distinction between the two pyrrolidine isomers, with the *R* isomer **24** exhibiting substantially improved oral exposure (AUC,u = 920 ng h mL^{-1}) compared with the *S* isomer **25** (AUC,u = 120 ng h mL^{-1}). In the PK study with pyrrolidine **25**, a steep tolerability threshold was observed. A 1 mg/kg iv dose was tolerated with no overt issues, but when a 3 mg/kg iv dose of **25** was administered, 3 of 3 mice died rapidly. Curiously, in spite of comparable exposure with iv dosing (data not shown), isomer **24** presented no obvious adverse events at 3 mg/kg. We initially hypothesized that the *S* isomer **25** may inhibit unidentified off-target kinases or receptors that could be responsible for the observed severe adverse events. However, off-target screening panel data failed to support this theory. For compound **25**, an internal panel of 19 receptors (see the Supporting Information) identified no hits (EC_{50} > 10 μM for all), and of 78 kinases tested (see the Supporting Information), only three resulted in <100-fold selectivity compared with PKCθ (Clk2, 6-fold; Cdk8, 6-fold; PKA, 19-fold).

In light of the unexplained toxicity observed with **25**, we turned our efforts toward the equipotent piperidine **26**. Because we had observed a significant amount of azetidine demethylation in our studies with methyl azetidine **11b**, we began routinely monitoring for both parent and desmethyl metabolite exposure in in vivo mouse PK studies. Typically the desmethyl metabolite and parent molecules had similar in vitro potency, as exemplified by **26** [PKCθ IC_{50} = 0.043 μM (parent) and 0.019 μM (metabolite); cellular IC_{50} = 0.20 μM (parent) and 0.19 μM (metabolite)], but the metabolite suffered from significantly reduced permeability [MDCK-MDR1 + CSA (pH 7.4) Papp A to B = 19 × 10^{-6} cm/s (parent) and 1.2 × 10^{-6} cm/s (metabolite)]. In general, a minimal shift in activity (~1- to 10-fold) between enzyme and cell assays were observed as long as the permeability remained greater than ~1 × 10^{-6} cm/s. In mouse PK, piperidine **26** exhibited low clearance (CL = 1.5 L h^{-1} kg^{-1}), resulting in a reasonable half-life ($t_{1/2}$ = 5.1 h). Oral bioavailability was good at 54%. Unbound oral AUC was 401 ng h mL^{-1} (10 mg/kg dose), and approximately 25% of the desmethyl metabolite (AUC,u = 56 ng h mL^{-1}) was observed.

dx.doi.org/10.1021/jm5013006 | J. Med. Chem. 2015, 58, 333–346

Consistent with good exposure, **26** inhibited IL-2 production in the Con A model (52 ± 4%, 10 mg/kg), on par with compound **1** (67 ± 3%, 10 mg/kg). Thus, the piperidine was established as a reasonable lead from which to improve potency in the context of favorable PK. An overlay of the polymethylated azetidine analogue (**11a**) with piperidine **26** highlighted the prospect of introducing methyl groups around the piperidine ring in order to occupy the van der Waals (VDW) space associated with the glycine-rich loop or toward the pre-DFG region (Figure 3) as a potential approach to improve potency. Cis methylation at the 3-position of the piperidine as in **17a** (the absolute structure was confirmed by small molecule X-ray analysis; see the Supporting Information for details) afforded desirable in vitro potency (PKCθ IC_{50} = 0.003 μM; IL-2 cell IC_{50} = 0.021 μM). Compound **17a** and desmethyl metabolite **27** had comparable activity, clearance, and unbound oral exposure (albeit ∼2-fold lower relative to parent **26**) and adequate half-life (Table 3). Approximately 10% of metabolite **27** was observed upon oral dosing of **17a**. In spite of similar in vitro and pharmacokinetic profiles, **17a** was more active (85 ± 3% inhibition, 10 mg/kg dose) than **27** (45 ± 7% inhibition, 10 mg/kg dose) in our screening Con A model, and thus, future analogues focused on tertiary amines. The cis stereoisomer of **17a**, compound **28**, also had compelling in vitro potency (IL-2 cell IC_{50} = 0.055 μM), notably higher oral exposure [AUC,u = 473 ng h mL^{-1} (parent) and 204 ng h mL^{-1} (metabolite)], and similar activity in the Con A model (85 ± 2% inhibition, 10 mg/kg dose). Dimethylation at the piperidine 3-position (**29**) was tolerated but provided no obvious advantage in terms of potency or PK. Piperidine *N*-ethylated derivative **30**, prepared in an attempt to fully block terminal dealkylation, yielded only moderately reduced in vivo clearance compared with parent **17a** (CL = 1.9 vs 3.3 L h^{-1} kg^{-1}) and no change in the amount of circulating dealkylated metabolite (∼11%).

A crystal structure in surrogate kinase PKCα (PDB accession code 4RA4) confirmed that the triazinone binding pose of **28** is similar to that of compound **11a** (Figure 4). As predicted, the piperidine N is in close contact with Asp481 (Asp522 in PKCθ). The *cis*-3-methyl substitution on the piperidine mimics the 3-methyl moiety on the azetidine in **11a**. In agreement with a lipophilic pocket identified in the crystal structure of **28** and consistent with our previous experience, a wide variety of substituents around the 7-aryl substituent were tolerated for in vitro potency (**17a–l**; Table 4). The C7 substituent therefore provided a convenient handle to modulate the PK properties.

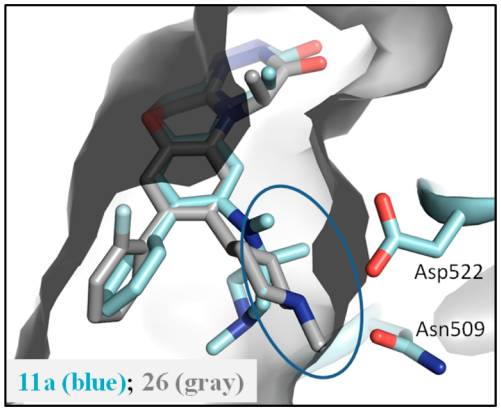

Figure 3. Overlay of the crystal structure of **11a** (blue) with a model of **26** (gray) in PKCθ, highlighting the lipophilic region for targeting with substitution on the 6-piperidine.

Table 3. Structure–Activity Relationships for Piperidine Ring Substitution

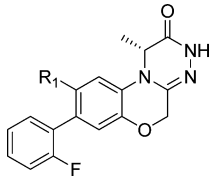

compd	**26**	**17a**	**27**	**28**	**29**[f]	**30**
R_1	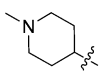	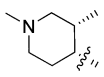	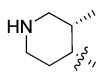	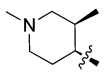	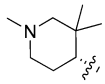	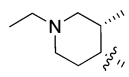
PKCθ IC_{50}[a] (μM)	0.043	0.003	0.004	0.016	0.003	0.005
IL-2 IC_{50}[a] (μM)	0.20	0.021	0.044	0.055	0.015	0.023
$CL_{int,u}$[b], hu/mu (L/h/kg)	6.2 / 38	9.9 / 56	9.2 / 27	9.5 / 29	17 / 179	8.8 / 70
CLp (L/h/kg)[c]	1.6	3.3	3.8	1.6	1.9	1.9
CLp,u (L/h/kg)[c]	14	23	21	12	39	24
t1/2 (h)[c]	5.1	3.8	9.7	2.9	2.6	1.8
Cmax,u (ng/mL)[c]	67.0	54.6	61.9	125	24.1	42.9
AUC,u parent (ng*h/mL)[c]	401	155	258	473	113	159
AUC,u metab. (ng*h/mL)[c,d]	56.3	17.4	--	204	30.1	19.0
F (%)[c]	54	32	53	53	39	38
Con A (% inhibition)[e]	52	85	45	85	73	75

[a]Means from $n \geq 2$ experiments. [b]In vivo predicted unbound CL_{int} from mouse and human microsome stability studies. [c]Mouse PK reported (3 mg/kg iv bolus in 50% PEG400; po dose of 10 mg/kg in 0.5% HPMC and 0.02% Tween80). Data are reported as averages of three animals. [d]AUC of desmethyl metabolite measured in the mouse PK study. [e]Compound was dosed at 10 mg/kg in mice 2 h prior to Con A challenge. Readout is % inhibition of IL-2 production. [f]The absolute stereochemistry at the 4-position of the piperidine was not determined but is proposed to be as drawn; the stereoisomeric compound had PKCθ IC_{50} = 0.19 μM.

dx.doi.org/10.1021/jm5013006 | J. Med. Chem. 2015, 58, 333–346

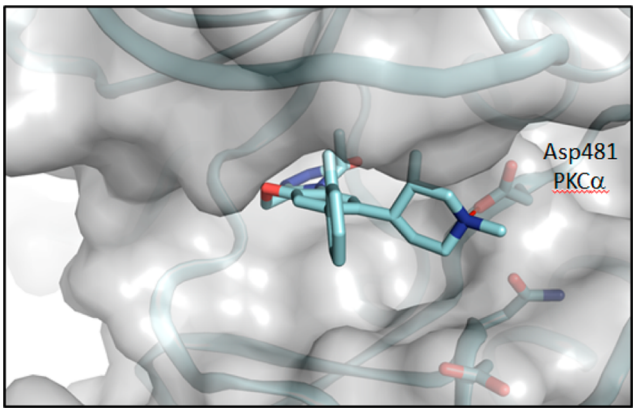

Figure 4. X-ray crystal structure of **28** in PKCα (PDB accession code 4RA4).

Previously we demonstrated that a drop in mean arterial pressure in rat and dog CV studies was observed with earlier analogues.[1] Our goal was to minimize the C_{max}/C_{min} ratio while achieving extended coverage over the unbound cellular EC_{80} in our chronic in vivo efficacy model by identifying compounds with a long half-life ($t_{1/2}$ > 5 h) and low unbound C_{max} ($C_{max,u}$ < 200 ng/mL). In PK studies, we observed that analogues of **17a** generally produced <10% of the corresponding desmethyl metabolites. Thus, in order to more rapidly prioritize compounds, a PK screening protocol (3 mg/kg iv bolus and po dose of 10 mg/kg) was utilized that eliminated metabolite measurement (Table 4). Fluorination of the aryl ring (**17a**–**c**) was tolerated, with a slight potency preference for 2-F substitution (**17a**), which gave a reasonable half-life ($t_{1/2}$ = 3.8 h) and $C_{max,u}$ (55 ng/mL). Substitution at the 4-position with either CH_3 (**17e**) or OCH_3 (**17g**) provided good in vitro potency and protracted half-life (8.5 and 9.6 h, respectively) with moderate $C_{max,u}$ values (17 and 91 ng/mL, respectively). The 2-CH_3 and 3-OCH_3 analogues (**17d** and **17f**), while tolerated in terms of PKCθ activity, had markedly shorter half-lives (3.3 and 1.6 h, respectively). Incorporation of a pyridyl ring, as in the crossover 5-(2-methoxy)pyridyl analogue (not shown), gave potency comparable to that of 4-methoxyphenyl derivative **17g** but with a higher $C_{max,u}$ (602 vs 91 ng/mL; data not shown) that was outside of our target criterion. The 3,4-dimethoxy analogue (**17i**) exhibited in a ∼10-fold loss in potency (IL-2 IC_{50} = 0.24 μM), while the analogous ethylenedioxy derivative **17j** retained good in vitro activity (IL-2 IC_{50} = 0.024 μM); apparently, the steric limitation of the 3,4-dimethoxy substitution could be resolved by conformational constraint (as in **17j**). However, this compound did not meet our target $t_{1/2}$ criterion with a moderate half-life ($t_{1/2}$ = 3.2 h). Combination of 2-F substitution with either the preferred 4-CH_3 or 4-OCH_3 group (**17k** and **17l**, respectively) provided excellent cellular potency (IL-2 cell IC_{50} = 0.010–0.014 μM) as well as a desirable half-life and low C_{max} ($t_{1/2}$ = 4.8 h and $C_{max,u}$ = 78 ng/mL for **17k**; $t_{1/2}$ = 11.6 h and $C_{max,u}$ = 113 ng/mL for **17l**). Both **17k** and **17l** inhibited IL-2 production in the Con A model (85 ± 3% and 86 ± 6%, respectively, 10 mg/kg dose).

Incorporation of two fluorine groups, as in 2,6-difluoro analogue **17h**, also gave excellent in vitro potency and activity in the acute Con A model (84 ± 3% inhibition of IL-2, 10 mg/kg dose). However, in a Con A dose–response study (at 1, 3, 10, and 30 mg/kg po), mortality occurred rapidly in several mice in the 30 mg/kg group, while tolerability issues in the 10 mg/kg group were not apparent. Although similar adverse events had been noted with pyrrolidine isomer **25** at a 3 mg/kg iv dose, this was the first instance where a single *oral* dose resulted in such a rapid and severe outcome. Because of the speed and severity of the effect, a profound impact on the cardiovascular system was suspected. In order to assess this hypothesis, compound **17h** was characterized in a conscious

Table 4. Structure–Activity Relationships of 7-Phenyl Substituents

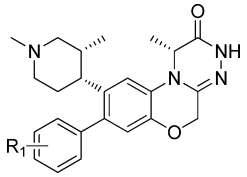

				mouse PK[b]			
compd	R_1	PKCθ IC_{50} (μM)[a]	IL-2 IC_{50} (μM)[a]	$t_{1/2}$ (h)	$C_{max,u}$ (ng/mL)	AUC,u (ng h mL^{-1})	Con A (% inhibition)[c]
17a	2-F	0.003	0.022	3.8	54.6	155	85
17b	3-F	0.014	0.060	–	–	–	–
17c	4-F	0.019	0.080	–	–	–	–
17d	2-CH_3	0.008	0.040	3.3	120	924	74
17e	4-CH_3	0.024	0.082	8.5	17.4	324	49
17f	3-OCH_3	0.007	0.049	1.6	39.8	73.9	69
17g	4-OCH_3	0.010	0.041	9.6	90.8	1290	82
17h	2,6-di-F	0.002	0.013	–	–	–	84[d]
17i	3,4-di-OCH_3	0.240	–	–	–	–	–
17j	3,4-OCH_2CH_2O-	0.005	0.024	3.2	96.2	856	68
17k	2-F-4-CH_3	0.002	0.010	4.8	78.0	1020	85
17l	2-F-4-OCH_3	0.002	0.014	11.6	113	1400	86

[a]Means from $n \geq 2$ experiments. [b]Mouse PK reported (3 mg/kg iv bolus in 50% PEG400; po dose of 10 mg/kg in 0.5% HPMC and 0.02% Tween80). Data are reported as averages of three animals. [c]Compound was dosed at 10 mg/kg in mice 2 h prior to Con A challenge. Readout is % inhibition of IL-2 production. [d]During a Con A dose–response experiment, 3 of 15 mice died rapidly when given a 30 mg/kg po dose; the 10 mg/kg po dose was tolerated without any overt adverse signs.

dx.doi.org/10.1021/jm5013006 | J. Med. Chem. 2015, 58, 333–346

mouse CV model (see the Supporting Information for protocol details). Oral administration of **17h** to telemetrized mice at 30 mg/kg produced a significant decrease in mean arterial pressure (MAP) to a maximum effect of −22 mmHg at the 2 h time point (Figure 5), which could help to explain the mortality observed in mice at 30 mg/kg in the Con A experiment

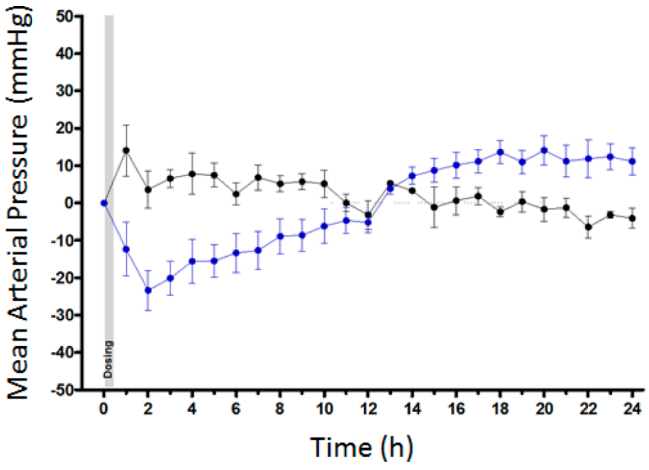

Figure 5. Conscious mouse CV data with **17h**. Blue dots: compound **17h**, po dose of 30 mg/kg in 0.5% HPMC and 0.02% Tween80 (n = 5). Black dots: vehicle (n = 5). Gray bar shows when compound **17h** was dosed.

Four compounds that did not display adverse effects (**17a**, **17k**, **17l**, and **28**) were selected for profiling in our internal kinome screening panel (Figure 6). Although the compounds displayed good overall selectivity, inhibition of PKA, Clk2, and Cdk8 was generally observed with these analogues bearing a 7-aryl substituent. When profiled in an internal bioprofiling panel that studies the functional effect of a compound on 19 receptors (see the Supporting Information for the receptors tested), compound **28** did not interact with any of the receptors at maximum concentrations of 10 μM. However, **17a** and **17k** both inhibited the L-type calcium channel (IC_{50} = 5.87 and 6.8 μM, respectively) and were agonists of the AT1 receptor (EC_{50} = 5.1 and 5.5 μM, respectively). In addition, **17k** and **17l** were evaluated in a battery of radioligand binding assays containing representatives of most G-protein-coupled receptors and a set of ligand and voltage-gated ion channel binding sites (CEREP; see the Supporting Information for the receptors tested). In addition to the receptors identified from internal testing, moderate interaction (50−75% inhibition at 10 μM) was observed with **17k** at the alpha1 receptor, M5 receptor, and the Na^{2+} current, and moderate interaction was observed with **17l** at the NK2 receptor and Na^{2+} current. Since all of the interactions with additional receptors were observed at concentrations greater than ~250-fold the PKCθ enzyme potency, the compounds were considered selective.

With compelling in vitro activity, an acceptable selectivity profile, and favorable PK profile, compound **17l** was selected for further profiling in the Con A model, giving dose responsive inhibition of IL-2 production [ED_{50} = 1.9 mg/kg (95% CI, 1.2−3.0 mg/kg); ED_{80} = 9.4 mg/kg (95% CI, 4.7−18.8 mg/kg)] (Figure 7). By comparison, a 10 mg/kg dose of **17a** was similarly effective, inhibiting IL-2 production at 85 ± 3%. Whereas **17a** unbound oral exposure was 153 ng/mL (1 h after dosing, just prior to Con A administration), the unbound

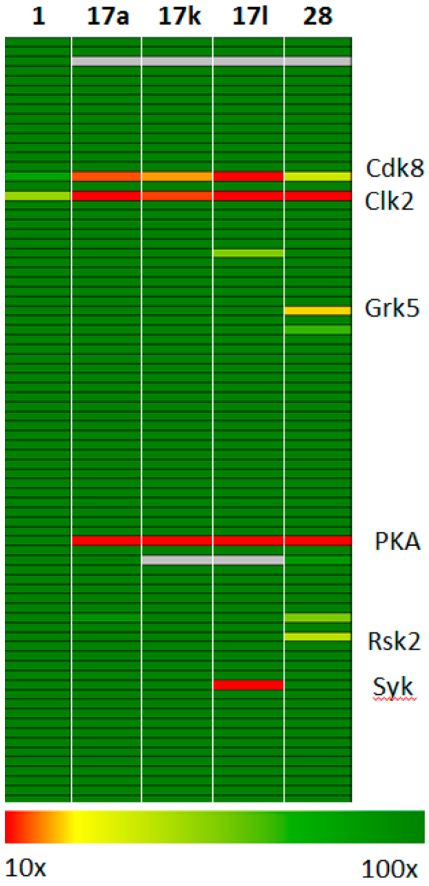

Figure 6. Comparison of kinome selectivity profiles of **1**, **17a**, **17k**, **17l**, and **28.** The kinome selectivity data are colored by fold selectivity over PKCθ IC_{50}, with ≤10-fold selective in red and a color gradient to ≥100-fold selective in green. Gray = not tested. Kinases with <40-fold selectivity are delineated on the right-hand side.

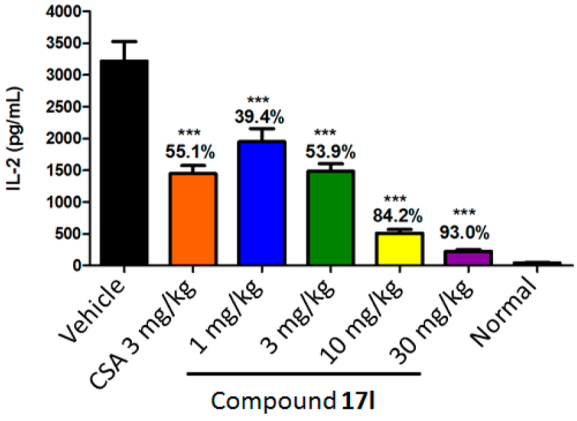

Figure 7. Acute in vivo activity (mouse Con A-induced IL-2 production) with **17l**. Mice were predosed orally with compound **17l** or 3 mg/kg cyclosporin A (CSA) 2 h prior to challenge. At 2 h postchallenge, serum was analyzed for murine IL-2 levels. Statistical significance was determined by one-way ANOVA using Dunnett's post-test.

exposure of **17l** was about 2.5-fold lower (66 ng/mL, 10 mg/kg dose). At t = 2 h after Con A administration (3 h after dosing), the exposure level of **17a** dropped significantly (total = 135 ng/mL; unbound = 20 ng/mL) while the exposure level of **17l** (10 mg/kg dose) was maintained (total = 664 ng/mL; unbound =

dx.doi.org/10.1021/jm5013006 | J. Med. Chem. 2015, 58, 333−346

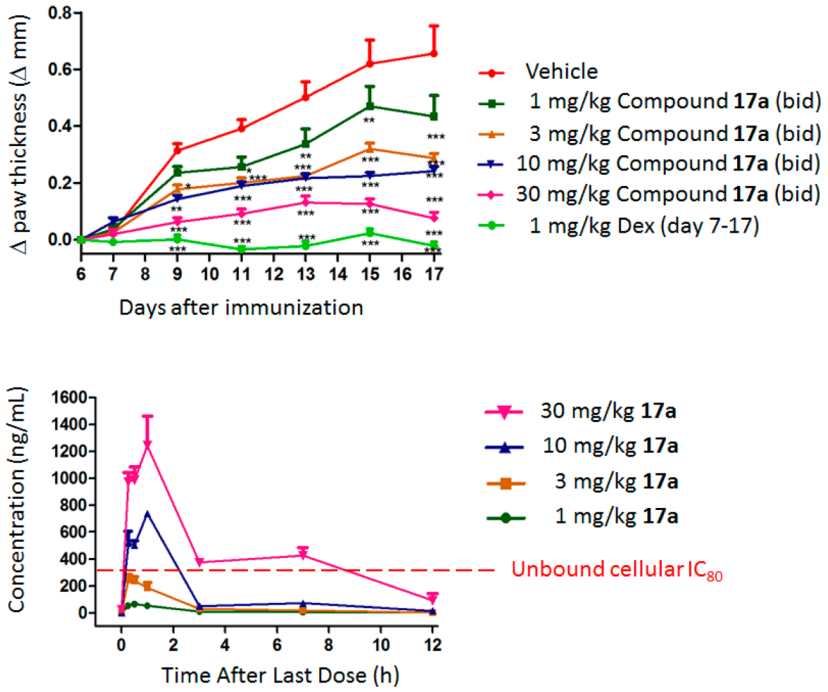

Figure 8. Chronic in vivo efficacy data (mouse GPI-induced arthritis model) and exposure data with prophylactic dosing of **17a**. GPI-immunized mice were dosed starting on day 0 with **17a** or with vehicle orally twice a day. Dexamethasone (Dex) was dosed orally starting on day 7. Statistical significance was determined by two-way ANOVA using a Bonferroni post-test. Terminal plasma exposures from the mouse GPI study were measured after the final dose on day 17 at 0, 0.25, 0.5, 1, 3, 7, and 12 h.

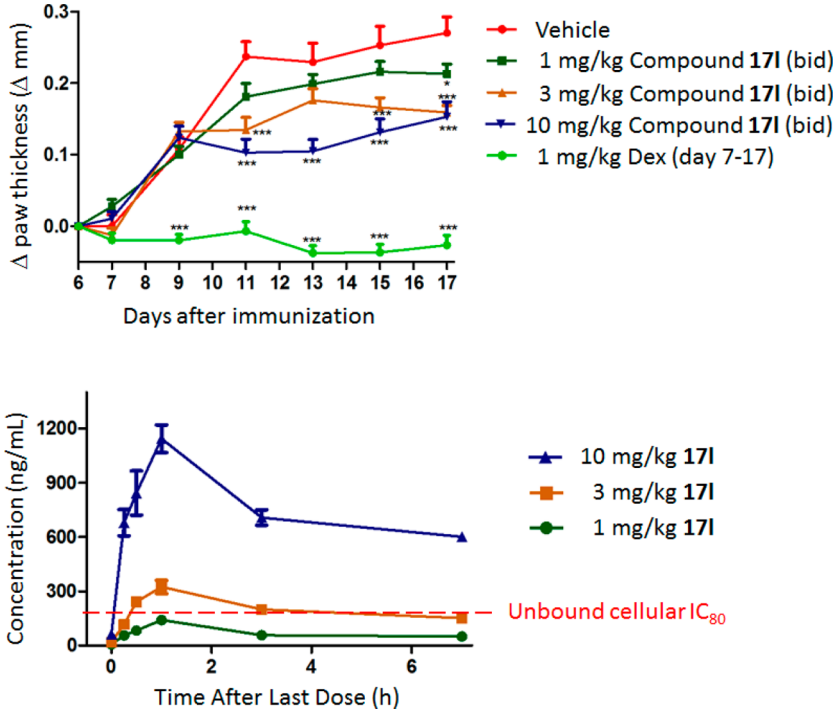

Figure 9. Chronic in vivo efficacy data (mouse GPI-induced arthritis model) and exposure data with prophylactic dosing of **17l**. GPI-immunized mice were dosed starting on day 0 with **17l** or with vehicle orally twice a day. Dexamethasone (Dex) was dosed orally starting on day 7. Statistical significance was determined by two-way ANOVA using a Bonferroni post-test. The 30 mg/kg group was terminated on day 4 because of severe side effects. Terminal plasma exposures from the mouse GPI study were measured after the final dose on day 17 at 0, 0.25, 0.5, 1, 3, 7, and 12 h. The 12 h time point for **17l** is not reported because of an apparent sample mixup.

111 ng/mL). Because of the comparable activities in spite of different exposure profiles and the short nature of the Con A model, these results suggest that activity in the acute model is C_{max}-driven.

To compare the effects of C_{max} versus time-over-target coverage in our chronic model, we hypothesized that 12 h coverage of the PKCθ unbound cellular IC_{80} would result in maximal efficacy. PK modeling with **17l** predicted that a 10

dx.doi.org/10.1021/jm5013006 | J. Med. Chem. 2015, 58, 333−346

mg/kg BID dose would fully cover the unbound cellular IC_{80} in the GPI model yet also maintain a minimal C_{max}, whereas a 30 mg/kg dose of **17a** was predicted to give ~6 h of coverage over the unbound cellular IC_{80}. Treatment with **17a** in the GPI model resulted in a full dose response, giving 77 ± 2% inhibition of paw swelling at the top dose (30 mg/kg). Coverage over the unbound cellular IC_{80} lasted for approximately 7 h. Similarly, administration of **17l** in the GPI model at 10 mg/kg gave extended coverage over the unbound cellular IC_{80}, but only partial efficacy (43% inhibition of paw swelling) was observed. With **17l**, the 30 mg/kg dose group had to be terminated on day 4; one animal was found dead and other mice were exhibiting convulsive behavior and were otherwise lethargic. However, no tolerability issue was seen with the 30 mg/kg cohort in the experiment with **17a**. On the basis of the exposure data with **17l**, simple time-over-target coverage of PKCθ appears insufficient for efficacy in this model of arthritis. Interestingly, the C_{max} with a 30 mg/kg dose of **17a** (Figure 8) was similar to that of the 10 mg/kg dose of **17l** (Figure 9), but at these doses **17a** was significantly more efficacious than **17l**. PKCα is known to play a role in T cell proliferation and differentiation, and thus, it could be expected to contribute to efficacy. Since inhibition of PKCα has been associated with increases in contractility as discussed in our previous paper,[1] we actively targeted minimal PKCα activity with our compounds in order to avoid introducing additional cardiovascular risk. In vitro, **17a** and **17l** inhibit PKCα to a comparable degree (IC_{50} = 0.31 μM for **17a** and 0.45 μM for **17l**), resulting in 90- and 200-fold selectivity margins, respectively. Thus, we cannot attribute the superior efficacy of **17a** to the contribution of PKCα inhibition. Other analogues tested in the GPI model demonstrated only partial efficacy, similar to **17l** (data not shown), in spite of compound levels sufficient for target coverage. We concluded that PKCθ inhibition alone is inadequate to give full efficacy in this chronic arthritis model, but we are still unable to rationalize the two exceptions (compounds **1** and **17a**) that resulted in full efficacy in the model.

In order to understand the genesis of the severe and rapid adverse events that were observed with compounds **1**, **17h**, **17l**, and **25**, the apparently well-tolerated compound **17a** was advanced to dose-escalating mouse PK (100 and 300 mg/kg doses) in preparation for a mouse toxicology study. Following a single dose of 100 or 300 mg/kg in the PK study, mice exhibited seizurelike activity, and all of the mice were found dead or were euthanized (within ~30 min at 300 mg/kg and 1−3 h at 100 mg/kg). Upon demonstration of sufficient exposure above the cellular IC_{80} with multiple compounds (exemplified by **17l**) that resulted in only partial efficacy in the GPI model and for lack of better understanding of the unpredictable nature of the adverse events observed with multiple triazinones, work with this chemotype on the PKCθ project targeting arthritic indications was halted.

CONCLUSION

The cocrystal structures of compound **11a** with PKCθ and the surrogate structure of compound **28** in PKCα guided a design-based effort to optimize the triazinone chemotype targeting reduced efficacious exposure through a combination of improved potency and optimal PK profile. A screening Con A model enabled the rapid prioritization of multiple analogues, ultimately leading to the identification of PKCθ inhibitors with improved cellular activity (IC_{50} < 0.025 μM) and good oral exposure with a low C_{max}/C_{min} ratio, as exemplified by compound **17l**. When advanced in vivo, in spite of full coverage over the unbound cellular IC_{80}, compound **17l** showed only marginal efficacy in the mouse GPI model, lending credence to the argument that inhibition of PKCθ alone may be insufficient for efficacy in this arthritis model. Multiple compounds (including **17l**) from the triazinone chemotype caused severe side effects, including death, in in vivo studies. Unable to definitively attribute these effects to a particular off-target kinase or receptor, work on this chemical matter was halted. Challenged with the inability to rationally design away from the severe toxicity effects combined with a lack of confidence in PKCθ as a target for arthritis, the PKCθ program effort was halted.

MATERIALS AND METHODS

Chemistry. All reagents and anhydrous solvents were of the highest grade available and were purchased from commercial sources and used without further purification or distillation, unless otherwise noted. All NMR spectra were recorded on Bruker Avance III 400 MHz FT-NMR spectrometer with a 5 mm BBO(F) probe or a Varian 400 MHz spectrometer with an $^{1}H/^{19}F/^{31}P/^{13}C$ 5 mm PFG 4Nuc probe. ^{1}H chemical shifts (δ) are reported in parts per million with MeOH-d_3, DMSO-d_6, or $CDCl_3$ as the reference standard. Data are reported as follows: chemical shift (multiplicity, coupling constant in hertz, integration). Multiplicities are denoted as follows: s = singlet, d = doublet, t = triplet, q = quartet, br = broad, m = multiplet. Analytical LC−MS analyses were conducted using Shimadzu LC-20AB pumps and an SPD-M20 PDA detector set at 220 and 254 nm, and the MS detection was performed with a MS-2010EV Micromass Platform LC spectrometer in electrospray ionization mode. Unless alternative column and eluting conditions are detailed in the experiment, the LC−MS method used was as follows. Column: Ultimate XB-C18, 3 μm, 30 mm × 2.1 mm. Mobile phase: acetonitrile (0.02% TFA) in water (0.04% TFA) from 10% to 80% within 4 min. Flow rate: 1.2 mL/min. Wavelength: 220 nm. Analytical SFC-MS analyses were conducted using Mettler pumps and an Agilent G1315B detector set at 190−370 nm, and the MS detection was performed with an Agilent 6110 detector following the detailed column and eluting conditions specified below. Preparative reversed-phase (RP) HPLC was performed using a Gilson 322 pump, a Gilson 156 UV detector set at 220 and 254 nm, and a Gilson GX-281 liquid handler, following the detailed column and eluting conditions specified below. Normal-phase silica gel preparative purification was performed using an automated Combiflash companion from ISCO with prepacked silica gel cartridges supplied by Santai Technologies Inc. and Agela Inc. SFC separation was performed using a Berger SFC Analytix system following the detailed column and eluting conditions specified below. Microwave reactions were performed using a Biotage INITIATOR60EXP microwave synthesis system. Qualitative (±) optical rotation data were collected using a PDR-chiral advanced laser in-line polarimeter (model ALP2002). Analytical thin-layer chromatography (TLC) was performed using SGF254 TLC plates (0.2−0.25 mm) supplied by Combinol Reagent (Yantai) Co., Ltd. Preparative TLC was performed using SGF254 TLC plates (0.4−0.5 mm) supplied by Yucheng Chemical (Shanghai) Co., Ltd. The purities of the final products were ≥95% as established by analytical liquid chromatography using a PDA detector at 220 nm and confirmed by ^{1}H NMR spectroscopy.

3-Methyl-4-trifluoromethanesulfonyloxy-3,6-dihydro-2*H*-pyridine-1-carboxylic Acid *tert*-Butyl Ester. To a mixture of 3-methyl-4-oxopiperidine-1-carboxylic acid *tert*-butyl ester (0.4 g, 1.876 mmol) in THF (5 mL) was added KHMDS (1 M in THF, 2.81 mL, 2.81 mmol) dropwise at −78 °C, and the reaction mixture was stirred for 30 min, allowed to warm to ambient temperature, and stirred for 3 h. The reaction mixture was cooled at −78 °C, and a solution of *N*-(5-chloropyridin-2-yl)-1,1,1-trifluoro-*N*-((trifluoromethyl)sulfonyl)-methanesulfonamide (0.884 g, 2.251 mmol) in THF (5 mL) was added dropwise. The reaction mixture was allowed to warm to

dx.doi.org/10.1021/jm5013006 | J. Med. Chem. 2015, 58, 333−346

ambient temperature and stirred overnight. Saturated aqueous NH_4Cl (20 mL) was added, and the reaction mixture was extracted with EtOAc (3 × 10 mL). The combined organic layers were washed with brine (20 mL), dried over Na_2SO_4, and concentrated in vacuo. The residue was purified by column chromatography on silica gel (eluting with 1−15% EtOAc in petroleum ether) to give 3-methyl-4-trifluoromethanesulfonyloxy-3,6-dihydro-2*H*-pyridine-1-carboxylic acid *tert*-butyl ester (0.31 g, 47%) as a colorless oil. TLC: R_f = 0.70 (eluting with 10% EtOAc in petroleum ether). ^{1}H NMR (400 MHz, $CDCl_3$): δ 5.73 (br s, 1H), 4.24−3.89 (m, 2H), 3.76−3.31 (m, 2H), 2.63 (br s, 1H), 1.48 (s, 9H), 1.16 (d, J = 7.0 Hz, 3H).

(*R*)-6-((3*R*,4*R*)-1,3-Dimethylpiperidin-4-yl)-7-(2-fluorophenyl)-4-methyl-2,10-dihydro-9-oxa-1,2,4a-triazaphenanthren-3-one Hydrochloride (17a). *Step A.* To a mixture of 2-amino-4-bromophenol (50 g, 266 mmol) and $NaHCO_3$ (67.0 g, 798 mmol) in water (200 mL) and DME (200 mL) was added 2-chloroacetyl chloride (45.1 g, 399 mmol) at 0 °C. The reaction mixture was stirred at 15 °C for 30 min and then heated at 80 °C overnight. The reaction mixture was cooled to ambient temperature and quenched with water (400 mL). The precipitate was collected by suction filtration, washed with water (200 mL) and petroleum ether (300 mL), and dried to give 6-bromo-4*H*-benzo[1,4]oxazin-3-one (59 g, 97%) as a gray solid. TLC: R_f = 0.24 (eluting with 30% EtOAc in petroleum ether). ^{1}H NMR (DMSO-d_6, 400 MHz): δ 7.07 (d, J = 8.4 Hz, 1H), 7.02 (s, 1H), 6.90 (d, J = 8.4 Hz, 1H), 4.59 (s, 2H).

Step B. To a mixture of 6-bromo-4*H*-benzo[1,4]oxazin-3-one (59 g, 259 mmol) in THF (800 mL) was added KHMDS (1 M in THF, 259 mL, 259 mmol) dropwise at 0 °C, and the reaction mixture was stirred for 30 min. (*S*)-Ethyl 2-(((trifluoromethyl)sulfonyl)oxy)propanoate[1] (117 g, 466 mmol) was added. The reaction mixture was warmed to ambient temperature and stirred for 2 h. The reaction mixture was quenched by the addition of water (1000 mL). The organic phase was separated, and the aqueous solution was extracted with EtOAc (4 × 500 mL). The combined organic phases were washed with brine (1 L), dried over Na_2SO_4, and concentrated in vacuo. The residue was purified by column chromatography on silica gel (eluting with 5−10% EtOAc in petroleum ether) to give (*R*)-2-(6-bromo-3-oxo-2,3-dihydrobenzo[1,4]oxazin-4-yl)propionic acid ethyl ester (82.4 g, 97%) as a brown liquid. TLC: R_f = 0.37 (eluting with 30% EtOAc in petroleum ether). ^{1}H NMR (400 MHz, $CDCl_3$): δ 7.12 (d, J = 8.8 Hz, 1H), 6.97 (s, 1H), 6.92 (d, J = 8.8 Hz, 1H), 5.23 (q, J = 6.8 Hz, 2H), 4.67−4.58 (d, J = 14.8 Hz, 2H), 4.26−4.20 (m, 2H), 1.60 (d, J = 6.8 Hz, 3H), 1.23 (t, J = 7.6 Hz, 3H). SFC (column, Chiralpak AD-H 250 mm × 4.6 mm i.d., 5 μm; mobile phase, MeOH (0.05% DEA) in supercritical CO_2 from 5% to 40%; flow rate, 2.35 mL/min; wavelength, 220 nm): t_R = 4.146 min. $[\alpha]_{20}^{D}$ 31.45 (c = 0.002 g/mL in MeOH).

Step C. A solution of (*R*)-2-(6-bromo-3-oxo-2,3-dihydrobenzo-[1,4]oxazin-4-yl)propionic acid ethyl ester (82.4 g, 252 mmol) and Lawesson reagent (61.1 g, 151 mmol) in toluene (900 mL) was heated at reflux for 3 h and then cooled to ambient temperature. The solvent was removed in vacuo, and the residue was purified by chromatography on silica gel (eluting with 5−10% EtOAc in petroleum ether) to give (*R*)-2-(6-bromo-3-thioxo-2,3-dihydrobenzo-[1,4]oxazin-4-yl)propionic acid ethyl ester (75.2 g, 87%) as a yellow solid. TLC: R_f = 0.55 (eluting with 12% EtOAc in petroleum ether). ^{1}H NMR (400 MHz, $CDCl_3$): δ 7.19 (d, J = 8.8 Hz, 1H), 7.04 (s, 1H), 6.93 (d, J = 8.8 Hz, 1H), 6.57 (m, 2H), 4.96−4.87 (m, 2H), 4.29−4.16 (m, 2H), 1.71 (d, J = 6.8 Hz, 3H), 1.18 (t, J = 6.8 Hz, 3H). SFC (column, Chiralpak AD-H 250 mm × 4.6 mm i.d., 5 μm; mobile phase, MeOH (0.05% DEA) in supercritical CO_2 from 5% to 40%; flow rate, 2.35 mL/min; wavelength, 220 nm): t_R = 3.529 min. $[\alpha]_{20}^{D}$ 19.25 (c = 0.002 g/mL in MeOH).

Step D. To a mixture of (*R*)-2-(6-bromo-3-thioxo-2,3-dihydrobenzo[1,4]oxazin-4-yl)propionic acid ethyl ester (75.2 g, 219 mmol) in EtOH (800 mL) was added hydrazine hydrate (98%, 21.9 g, 438 mmol), and the reaction mixture was stirred at ambient temperature overnight. The precipitate was collected by filtration and washed with cold EtOH (3 × 80 mL) to give 6-bromo-4-methyl-2,10-dihydro-9-oxa-1,2,4a-triazaphenanthren-3-one (6 g, 9%) as a yellow solid. The filtrate was concentrated to give an additional 70 g of crude product, which was purified by chromatography on silica gel (eluting with 10−25% EtOAc in petroleum ether) to give a second batch of (*R*)-6-bromo-4-methyl-2,10-dihydro-9-oxa-1,2,4a-triazaphenanthren-3-one (45.9 g, 71%) as a yellow solid. ^{1}H NMR (400 MHz, $CDCl_3$): δ 8.53 (br s, 1H), 7.10 (d, J = 8.4 Hz, 1H), 7.03 (s, 1H), 6.89 (d, J = 8.4 Hz, 1H), 4.69−4.52 (m, 3H), 1.52 (d, J = 6.8 Hz, 3H). LC−MS (column, Ultimate XB-C18, 3 μm, 30 mm × 2.1 mm; mobile phase, acetonitrile (0.02% TFA) in water (0.04% TFA) from 5% to 95% within 1.5 min; flow rate, 1.2 mL/min; wavelength, 220 nm): t_R = 0.745 min. MS: m/z 297 $[M + H]^+$. SFC (column, Chiralpak AS-H 250 mm × 4.6 mm i.d., 5 μm; mobile phase, EtOH (0.05% DEA) in supercritical CO_2 from 5% to 40%; flow rate, 2.35 mL/min; wavelength, 220 nm): t_R = 6.075 min. $[\alpha]_{20}^{D}$ −314.92 (c = 0.002 g/mL in MeOH).

Step E. To a mixture of 3-methyl-4-trifluoromethanesulfonyloxy-3,6-dihydro-2*H*-pyridine-1-carboxylic acid *tert*-butyl ester (5.07 g, 14.69 mmol), (*R*)-4-methyl-6-(4,4,5,5-tetramethyl[1,3,2]-dioxaborolan-2-yl)-2,10-dihydro-9-oxa-1,2,4a-triazaphenanthren-3-one[2] (2.8 g, 8.16 mmol), and K_3PO_4 (3.46 g, 16.32 mmol) in DMF (60 mL) and water (10 mL) was added $Pd(Ph_3P)_4$ (3.77 g, 3.26 mmol). The reaction mixture was stirred at 80 °C overnight and then cooled to ambient temperature and concentrated in vacuo. The residue was purified by column chromatography on silica gel (eluting with 3−50% EtOAc in petroleum ether) to give a yellow liquid (3.5 g). Further purification by preparative HPLC (column, Agella Venusil ASB 150 mm × 25 mm, 5 μm; mobile phase, acetonitrile in water (0.05% HCl) from 50% to 75% in 12 min; flow rate, 30 mL/min; wavelength, 220 nm) gave 3-methyl-4-((*R*)-4-methyl-3-oxo-2,3,4,10-tetrahydro-9-oxa-1,2,4a-triazaphenanthren-6-yl)-3,6-dihydro-2*H*-pyridine-1-carboxylic acid *tert*-butyl ester (1.5 g, 44%) as a white solid. ^{1}H NMR (400 MHz, $CDCl_3$): δ 8.03 (br s, 1H), 7.02−6.93 (m, 2H), 6.87 (s, 1H), 5.81 (br s, 1H), 4.77 (q, J = 6.8 Hz, 1H), 4.59 (d, J = 13.2 Hz, 2H), 4.47−4.18 (m, 1H), 3.95−3.77 (m, 2H), 3.32 (d, J = 13.2 Hz, 1H), 2.79 (br s, 1H), 1.53 (m, 3H), 1.51 (s, 9H), 1.02 (d, J = 6.8 Hz, 3H). LC−MS (column, Ultimate XB-C18, 3 μm, 30 mm × 2.1 mm; mobile phase, MeCN (0.02% TFA) in water (0.04% TFA) from 10% to 80% within 7 min; flow rate, 1.2 mL/min; wavelength, 220 nm): t_R = 3.339 min. MS: m/z 413 $[M + H]^+$. The isomers were separated by chiral SFC (column, Chiralpak AD 300 mm × 50 mm i.d., 10 μm; mobile phase, supercritical CO_2/EtOH (0.1% $NH_3 \cdot H_2O$) = 60/40; flow rate, 220 mL/min; wavelength, 220 nm) to give (*R*)-3-methyl-4-((*R*)-4-methyl-3-oxo-2,3,4,10-tetrahydro-9-oxa-1,2,4a-triazaphenanthren-6-yl)-3,6-dihydro-2*H*-pyridine-1-carboxylic acid *tert*-butyl ester (isomer 1) as a white solid (0.57 g, 38%; SFC (column, Chiralcel OJ-H 250 mm × 4.6 mm i.d., 5 μm; mobile phase, MeOH (0.05% DEA)/supercritical CO_2 from 5% to 40%; flow rate, 2.35 mL/min; wavelength, 220 nm): t_R = 8.56 min). ^{1}H NMR (400 MHz, $CDCl_3$): δ 8.03 (br s, 1H), 6.99−6.94 (m, 2H), 6.86 (s, 1H), 5.81 (d, J = 15.6 Hz, 1H), 4.77 (q, J = 6.6 Hz, 1H), 4.67−4.53 (m, 2H), 3.85 (dd, J = 3.3, 13.1 Hz, 2H), 3.31 (dd, J = 3.9, 12.9 Hz, 1H), 2.79 (br s, 1H), 1.55 (d, J = 6.8 Hz, 3H), 1.51 (s, 9H), 1.02 (d, J = 6.8 Hz, 3H). LC−MS (column, Ultimate XB-C18, 3 μm, 30 mm × 2.1 mm; mobile phase, acetonitrile (0.02% TFA) in water (0.04% TFA) from 5% to 95% within 1.5 min; flow rate, 1.2 mL/min; wavelength, 220 nm): t_R = 0.869 min. MS: m/z 413 $[M + H]^+$. (*S*)-3-methyl-4-((*R*)-4-methyl-3-oxo-2,3,4,10-tetrahydro-9-oxa-1,2,4a-triazaphenanthren-6-yl)-3,6-dihydro-2*H*-pyridine-1-carboxylic acid *tert*-butyl ester (isomer 2) was also obtained as a white solid (0.57 g, 38%; SFC (column, Chiralcel OJ-H 250 mm × 4.6 mm i.d., 5 μm; mobile phase, MeOH (0.05% DEA)/supercritical CO_2 from 5% to 40%; flow rate, 2.35 mL/min; wavelength, 220 nm): t_R = 6.86 min). ^{1}H NMR ($CDCl_3$, 400 MHz): δ 8.08 (br s, 1H), 7.01−6.93 (m, 2H), 6.87 (s, 1H), 5.82 (br s, 1H), 4.77 (q, J = 6.6 Hz, 1H), 4.60 (q, J = 13.1 Hz, 2H), 4.47−4.13 (m, 1H), 3.85 (dd, J = 3.0, 12.8 Hz, 2H), 3.32 (dd, J = 3.4, 12.9 Hz, 1H), 2.78 (br s, 1H), 1.55−1.51 (m, 3H), 1.51 (s, 9H), 1.02 (d, J = 6.8 Hz, 3H). LC−MS (column, Ultimate XB-C18, 3 μm, 30 mm × 2.1 mm; mobile phase, acetonitrile (0.02% TFA) in water (0.04% TFA) from 5% to 95% within 1.5 min; flow rate, 1.2 mL/min; wavelength, 220 nm): t_R = 0.869 min. MS: m/z 413 $[M + H]^+$.

dx.doi.org/10.1021/jm5013006 | J. Med. Chem. 2015, 58, 333−346

Step F. A mixture of (*R*)-3-methyl-4-((*R*)-4-methyl-3-oxo-2,3,4,10-tetrahydro-9-oxa-1,2,4a-triazaphenanthren-6-yl)-3,6-dihydro-2*H*-pyridine-1-carboxylic acid *tert*-butyl ester (isomer 1, 0.55 g, 1.333 mmol) and Pd/C (10%, 0.142 g, 0.13 mmol) in MeOH (20 mL) was stirred under an atmosphere of H_2 (1 atm) at ambient temperature for 3 h. The reaction mixture was filtered, and the filtrate was concentrated in vacuo to give (3*R*,4*R*)-3-methyl-4-((*R*)-4-methyl-3-oxo-2,3,4,10-tetrahydro-9-oxa-1,2,4a-triazaphenanthren-6-yl)piperidine-1-carboxylic acid *tert*-butyl ester (0.54 g, 98%) as a colorless solid. ^{1}H NMR (400 MHz, $CDCl_3$) δ 8.35 (s, 1H), 6.97 (d, J = 8.4 Hz, 1H), 6.79 (d, J = 8.4 Hz, 1H), 6.71 (s, 1H), 4.77 (q, J = 6.8 Hz, 1H), 4.65−4.52 (d, J = 13.2 Hz, 2H), 4.48−3.98 (m, 2H), 3.18−2.73 (m, 3H), 2.13−1.92 (m, 2H), 1.61 (br s, 1H), 1.55−1.48 (m, 13H), 0.76−0.67 (d, J = 5.6 Hz, 3H). LC−MS (column, Merck, 3 μm, 25 mm × 2 mm; mobile phase, MeCN (0.02% TFA) in water (0.04% TFA) from 5% to 95% within 0.7 min, keep at 95% for 0.4 min, keep at 5% within 0.4 min; flow rate, 1.5 mL/min; wavelength, 220 nm): t_R = 0.869 min. MS: m/z 415 $[M + H]^+$. SFC (column, Chiralcel OD-3 150 mm × 4.6 mm i.d., 3 μm; mobile phase, EtOH (0.05% DEA)/supercritical CO_2 from 5% to 40%; flow rate, 2.5 mL/min; wavelength, 220 nm): t_R = 4.910 min.

Step G. To a mixture of (3*R*,4*R*)-3-methyl-4-((*R*)-4-methyl-3-oxo-2,3,4,10-tetrahydro-9-oxa-1,2,4a-triazaphenanthren-6-yl)piperidine-1-carboxylic acid *tert*-butyl ester (0.2 g, 0.483 mmol) in DCM (20 mL) and MeOH (10 mL) was added tetra-*N*-butylammonium tribromide (0.233 g, 0.483 mmol), and the reaction mixture was stirred at ambient temperature for 30 min. Saturated aqueous $Na_2S_2O_3$ (6 mL) was added, and the reaction mixture was extracted with DCM (4 × 10 mL). The combined organic phases were washed with brine (30 mL), dried over Na_2SO_4, and concentrated in vacuo. The residue was purified by preparative TLC (eluting with 50% EtOAc in petroleum ether) to give (3*R*,4*R*)-4-((*R*)-7-bromo-4-methyl-3-oxo-2,3,4,10-tetrahydro-9-oxa-1,2,4a-triazaphenanthren-6-yl)-3-methylpiperidine-1-carboxylic acid *tert*-butyl ester (0.12 g, 50%) as a colorless solid. ^{1}H NMR (400 MHz, CD_3OD): δ 7.23 (s, 1H), 6.84 (s, 1H), 4.87−4.81 (m, 1H), 4.64−4.54 (m, 2H), 4.32 (d, J = 12.8 Hz, 1H), 4.05 (d, J = 13.2 Hz, 1H), 3.20−2.75 (m, 3H), 2.37−2.17 (m, 3H), 1.48 (s, 9H), 1.44−1.38 (m, 4H), 0.73 (d, J = 6.8 Hz, 3H). LC−MS (column, Merck, 3 μm, 25 mm × 2 mm; mobile phase, MeCN (0.02% TFA) in water (0.04% TFA) from 5% to 95% within 0.7 min, keep at 95% for 0.4 min, keep at 5% within 0.4 min; flow rate, 1.5 mL/min; wavelength, 220 nm): t_R = 0.934 min. MS: m/z 493 $[M + H]^+$, 495 $[M + H + 2]^+$. SFC (column, Chiralpak AD-3, 150 mm × 4.6 mm i.d., 3 μm; mobile phase, MeOH (0.05% DEA) in supercritical CO_2 from 5% to 40%; flow rate, 2.5 mL/min; wavelength, 220 nm): t_R = 6.79 min.

Step H. To a mixture of (2-fluorophenyl)boronic acid (0.051 g, 0.365 mmol), (3*R*,4*R*)-4-((*R*)-7-bromo-4-methyl-3-oxo-2,3,4,10-tetrahydro-9-oxa-1,2,4a-triazaphenanthren-6-yl)-3-methylpiperidine-1-carboxylic acid *tert*-butyl ester (0.12 g, 0.243 mmol), and K_2CO_3 (0.067 g, 0.486 mmol) in 1,4-dioxane (12 mL) and water (2 mL) was added $PdCl_2$(dppf)−CH_2Cl_2 adduct (0.020 g, 0.024 mmol), and the reaction mixture was stirred at 90 °C overnight. The reaction mixture was cooled to ambient temperature and concentrated in vacuo, and the residue was purified by column chromatography on silica gel (eluting with 3−30% EtOAc in petroleum ether) to give (3*R*,4*R*)-4-[(*R*)-7-(2-fluorophenyl)-4-methyl-3-oxo-2,3,4,10-tetrahydro-9-oxa-1,2,4a-triazaphenanthren-6-yl]-3-methylpiperidine-1-carboxylic acid *tert*-butyl ester (0.076 g, 61%) as a colorless solid. ^{1}H NMR ($CDCl_3$, 400 MHz): δ 8.34 (br s, 1H), 7.44−7.32 (m, 1H), 7.24−7.11 (m, 3H), 6.85 (s, 1H), 6.73 (br s, 1H), 4.80 (br s, 1H), 4.70−4.53 (m, 2H), 4.43−4.17 (m, 1H), 3.90−3.60 (m, 1H), 2.89 (br s, 1H), 2.60 (br s, 2H), 1.56 (d, J = 6.8 Hz, 3H), 1.46 (m, 10H), 0.72 (m, 3H). LC−MS (column, Merck, 3 μm, 25 mm × 2 mm; mobile phase, MeCN (0.02% TFA) in water (0.04% TFA) from 5% to 95% within 0.7 min, keep at 95% for 0.4 min, keep at 5% within 0.4 min; flow rate, 1.5 mL/min; wavelength, 220 nm): t_R = 0.948 min. MS: m/z 509 $[M + H]^+$. SFC (column, Chiralpak AD-3, 150 mm × 4.6 mm i.d., 3 μm; mobile phase, MeOH (0.05% DEA) in supercritical CO_2 from 5% to 40%; flow rate, 2.5 mL/min; wavelength, 310 nm): t_R = 6.21 min.

Step I. A mixture of (3*R*,4*R*)-4-[(*R*)-7-(2-fluorophenyl)-4-methyl-3-oxo-2,3,4,10-tetrahydro-9-oxa-1,2,4a-triazaphenanthren-6-yl]-3-methylpiperidine-1-carboxylic acid *tert*-butyl ester (0.076 g, 0.149 mmol) in HCl (4 M in EtOAc, 15 mL) was stirred at ambient temperature for 1 h. The reaction mixture was concentrated in vacuo to give (*R*)-7-(2-fluorophenyl)-4-methyl-6-((3*R*,4*R*)-3-methylpiperidin-4-yl)-2,10-dihydro-9-oxa-1,2,4a-triazaphenanthren-3-one hydrochloride (**27**) (0.065 g, 98%) as a white solid. ^{1}H NMR (400 MHz, CD_3OD): δ 7.50−7.41 (m, 1H), 7.32−7.19 (m, 3H), 6.91 (br s, 1H), 6.86 (s, 1H), 4.80 (m, 1H), 4.70−4.59 (m, 2H), 3.48 (m, 1H), 3.15−2.98 (m, 2H), 2.82 (m, 1H), 2.43 (m, 1H), 1.88 (m, 2H), 1.50 (d, J = 6.4 Hz, 3H), 0.91 (br s, 3H). LC−MS: t_R = 1.534 min. MS: m/z 409 $[M + H]^+$. SFC (column, Chiralpak AS-H, 150 mm × 4.6 mm i.d., 5 μm; mobile phase, MeOH (0.05% DEA) in supercritical CO_2 from 5% to 40%; flow rate, 3 mL/min; wavelength, 220 nm): t_R = 1.341 min.

Step J. A mixture of (*R*)-7-(2-fluorophenyl)-4-methyl-6-((3*R*,4*R*)-3-methylpiperidin-4-yl)-2,10-dihydro-9-oxa-1,2,4a-triazaphenanthren-3-one hydrochloride (3.05 g, 6.88 mmol) and paraformaldehyde (2.066 g, 68.8 mmol) in MeOH (60 mL) and AcOH (6 mL) was stirred at 80 °C for 16 h. Sodium cyanoborohydride (0.865 g, 13.76 mmol) was added, and the reaction mixture was stirred at ambient temperature for 0.5 h. The reaction mixture was concentrated in vacuo, and the residue was purified by column chromatography on basicified silica gel (eluting with 10% MeOH in DCM) to give (*R*)-6-((3*R*,4*R*)-1,3-dimethylpiperidin-4-yl)-7-(2-fluorophenyl)-4-methyl-2,10-dihydro-9-oxa-1,2,4a-triazaphenanthren-3-one (1.15 g, 40%) as a white solid. The solid was stirred in HCl (4 M in EtOAc, 50 mL) for 30 min, and the reaction mixture was concentrated in vacuo to give (*R*)-6-((3*R*,4*R*)-1,3-dimethylpiperidin-4-yl)-7-(2-fluorophenyl)-4-methyl-2,10-dihydro-9-oxa-1,2,4a-triazaphenanthren-3-one hydrochloride (**17a**) (1.215 g, 39%) as a white solid. ^{1}H NMR (400 MHz, CD_3OD): δ 7.44 (m, 1H), 7.32−7.16 (m, 3H), 6.90 (m, 1H), 6.84 (s, 1H), 4.62 (d, J = 13.2 Hz, 2H), 3.57 (m, 1H), 3.25 (m, 1H), 3.05 (m, 2H), 2.86 (m, 1H), 2.79 (s, 3H), 2.50 (m, 1H), 1.91 (m, 2H), 1.48 (d, J = 6.8 Hz, 3H), 0.91 (m, 3H). LC−MS (column, Ultimate XB-C18, 3 μm; 30 mm × 2.1 mm; mobile phase, MeCN (0.02% TFA) in water (0.04% TFA) from 0% to 60% within 4 min; flow rate, 1.2 mL/min; wavelength, 220 nm): t_R = 2.275 min. MS: m/z 423 $[M + H]^+$. SFC (column, Chiralcel OJ-3, 50 mm × 4.6 mm i.d., 3 μm; mobile phase, MeOH (0.05% DEA) in supercritical CO_2 from 5% to 40%; flow rate, 4 mL/min; wavelength, 220 nm): t_R = 1.145 min.

(*R*)-6-((3*S*,4*S*)-1,3-Dimethylpiperidin-4-yl)-7-(2-fluorophenyl)-4-methyl-2,10-dihydro-9-oxa-1,2,4a-triazaphenanthren-3-one Hydrochloride (28). Prepared according to the procedure for compound **17a** (steps F−J). Step F: using (*S*)-3-methyl-4-((*R*)-4-methyl-3-oxo-2,3,4,10-tetrahydro-9-oxa-1,2,4a-triazaphenanthren-6-yl)-3,6-dihydro-2*H*-pyridine-1-carboxylic acid *tert*-butyl ester (the intermediate obtained in step E during the preparation of compound **17a**). Step G: tetra-*N*-butylammonium tribromide (1 equiv). Step H: (2-fluorophenyl)boronic acid (1.5 equiv), 90 °C overnight. Step I: HCl (4 M in EtOAc) at ambient temperature. Step J: paraformaldehyde (2.5 equiv) then sodium cyanoborohydride (2 equiv) in 3% overall yield as a white solid. ^{1}H NMR (400 MHz, MeOH-d_4): δ 7.49−7.40 (m, 1H), 7.33−7.17 (m, 3H), 6.91 (s, 1H), 6.85 (s, 1H), 4.99−4.93 (m, 1H), 4.70−4.65 (m, 2H), 3.60−3.50 (m, 1H), 3.25−3.00 (m, 3H), 2.90−2.85 (m, 1H), 2.80 (s, 3H), 2.55−2.45 (m, 1H), 2.01−1.84 (m, 2H), 1.49 (d, J = 6.4 Hz, 3H), 1.00−0.90 (m, 3H). LC−MS (at wavelengths of 220 and 254 nm): t_R = 1.654 min. MS: m/z 423 $[M + H]^+$. SFC (column, Chiralpak AS-H, 150 mm × 4.6 mm i.d., 5 μm; mobile phase, EtOH (0.05% DEA) in supercritical CO_2 from 5% to 40%; flow rate, 3 mL/min; wavelength, 220 nm): t_R = 3.206 min.

(*R*)-6-((3*R*,4*R*)-1,3-Dimethylpiperidin-4-yl)-7-(2-fluoro-4-methoxyphenyl)-4-methyl-2,10-dihydro-9-oxa-1,2,4a-triazaphenanthren-3-one (17l). *Step A.* A solution of (3*R*,4*R*)-4-((*R*)-7-bromo-4-methyl-3-oxo-2,3,4,10-tetrahydro-9-oxa-1,2,4a-triazaphenanthren-6-yl)-3-methylpiperidine-1-carboxylic acid *tert*-butyl ester (3 g, 6.08 mmol) in HCl (4 M in EtOAc, 10 mL) was stirred at ambient temperature for 1 h. The solvent was removed in vacuo to give crude (*R*)-7-bromo-4-methyl-6-((3*R*,4*R*)-3-methylpiperidin-4-yl)-2,10-dihydro-9-oxa-1,2,4a-triazaphenanthren-3-one hydrochloride (2.2 g, 82%) as a white solid, which was used directly in the next step. LC−MS

dx.doi.org/10.1021/jm5013006 | *J. Med. Chem.* 2015, 58, 333−346

(column, Merck, 3 μm, 25 mm × 2 mm; mobile phase, MeCN (0.02% TFA) in water (0.04% TFA) from 5% to 95% within 0.7 min, keep at 95% for 0.4 min, keep at 5% within 0.4 min; flow rate, 1.5 mL/min; wavelength, 220 nm): t_R = 0.720 min. MS: m/z 393 $[M + H]^+$, 395 $[M + H + 2]^+$.

Step B. To a solution of (*R*)-7-bromo-4-methyl-6-((3*R*,4*R*)-3-methylpiperidin-4-yl)-2,10-dihydro-9-oxa-1,2,4a-triazaphenanthren-3-one hydrochloride (2.2 g, 5.59 mmol) in AcOH (10 mL) and MeOH (100 mL) was added paraformaldehyde (0.839 g, 28.0 mmol). The reaction mixture was stirred at ambient temperature for 1 h. $NaBH_3CN$ (0.557 g, 14.0 mmol) was added, and the reaction mixture was stirred at ambient temperature overnight. Saturated aqueous $NaHCO_3$ (30 mL) was added, and the reaction mixture was extracted with EtOAc (3 × 50 mL). The combined organic phases were dried over sodium sulfate, filtered, and concentrated in vacuo. The residue was purified by preparatory HPLC (column, Phenomenex Gemini C18 200 mm × 25 mm, 10 μm; mobile phase, acetonitrile in water (0.1% TFA) from 20% to 45% in 10 min; flow rate, 25 mL/min; wavelength, 220 nm) to give (*R*)-7-bromo-6-((3*R*,4*R*)-1,3-dimethylpiperidin-4-yl)-4-methyl-2,10-dihydro-9-oxa-1,2,4a-triazaphenanthren-3-one (1.8 g, 79%) as a light-yellow solid. ^{1}H NMR (400 MHz, CD_3OD): δ 7.22 (s, 1H), 6.86 (s, 1H), 4.87−4.91 (m, 1H), 4.58 (d, J = 13.2 Hz, 2H), 3.15 (m, 1H), 3.04 (m, 1H), 2.84 (m, 1H), 2.23−2.39 (m, 6H), 2.07−2.18 (m, 1H), 1.55 (m, 1H), 1.43 (d, J = 6.5 Hz, 3H), 0.83 (d, J = 7.0 Hz, 3H). LC−MS (column, Merck, 3 μm, 25 mm × 2 mm; mobile phase, MeCN (0.02% TFA) in water (0.04% TFA) from 5% to 95% within 0.7 min, keep at 95% for 0.4 min, keep at 5% within 0.4 min; flow rate, 1.5 mL/min; wavelength, 220 nm): t_R = 0.681 min. MS: m/z 407 $[M + H]^+$, 409 $[M + H + 2]^+$.

Step C. To a mixture of (*R*)-7-bromo-6-((3*R*,4*R*)-1,3-dimethylpiperidin-4-yl)-4-methyl-2,10-dihydro-9-oxa-1,2,4a-triazaphenanthren-3-one (0.050 g, 0.123 mmol), (2-fluoro-4-methoxyphenyl)boronic acid (0.025 g, 0.147 mmol), and potassium carbonate (0.034 g, 0.246 mmol) in 1,4-dioxane (6 mL) and water (1 mL) was added $PdCl_2$(dppf)−CH_2Cl_2 adduct (0.020 g, 0.025 mmol), and the reaction mixture was heated at 90 °C overnight. The reaction mixture was cooled to ambient temperature and concentrated in vacuo. The residue was purified by column chromatography on silica gel (eluting with 10% MeOH in dichloromethane) to give (*R*)-6-((3*R*,4*R*)-1,3-dimethylpiperidin-4-yl)-7-(2-fluoro-4-methoxyphenyl)-4-methyl-2,10-dihydro-9-oxa-1,2,4a-triazaphenanthren-3-one (**17l**) (0.050 g, 90%) as a brown solid. LC−MS: t_R = 1.726 min. MS: m/z 453 $[M + H]^+$. ^{1}H NMR (400 MHz, CD_3OD): δ 7.18 (t, J = 8.5 Hz, 1H), 6.94−6.79 (m, 4H), 4.96−4.94 (m, 1H), 4.64 (d, J = 6.3 Hz, 2H), 3.86 (s, 3H), 3.51 (m, 1H), 3.24−2.78 (m, 4H), 2.74 (s, 3H), 2.48 (m, 1H), 2.00−1.82 (m, 2H), 1.50 (d, J = 6.5 Hz, 3H), 0.91 (d, J = 7.3 Hz, 3H). SFC (column, Chiralpak AS-H, 150 mm × 4.6 mm i.d., 5 μm; mobile phase, MeOH (0.05% DEA) in supercritical CO_2 from 5% to 40%; flow rate, 3 mL/min; wavelength, 220 nm): t_R = 3.175 min.

Biology. Kinase and cellular assays and Con A and GPI in vivo models were run following protocols described previously.[1] To enable higher throughput, a modified screening version of the Con A model was utilized in which each compound was tested at a single 10 mg/kg dose rather than in dose−response format. This allowed preliminary analysis of up to five compounds per experiment wherein compounds were dosed 1 h prior to challenge (t = −1 h), an orbital bleed for an estimated C_{max} was taken immediately prior to Con A administration (t = 0 h), and 2 h later (t = 2 h) IL-2 levels and terminal compound concentrations were measured.

■ ASSOCIATED CONTENT

Ⓢ Supporting Information

Additional experimental details. This material is available free of charge via the Internet at http://pubs.acs.org.

■ AUTHOR INFORMATION

Corresponding Author

*Telephone: 1-508-688-8001. E-mail: dawn.george@abbvie.com.

Author Contributions

The manuscript was written through contributions of all authors. All authors have given approval to the final version of the manuscript. D.M.G., E.C.B., M.A.A., P.B.-P., D.B.D., P.H., Q.L., S.M., L.R., A.S., and J.J.E. are employees at AbbVie. The design, study conduct, and financial support for the research were provided by AbbVie. Y.Z., J.W., and J.S. are employees at WuXi AppTec (Shanghai) Co., Ltd. AbbVie and WuXi participated in the interpretation of data, review, and approval of the publication.

Notes

The authors declare no competing financial interest.

■ ACKNOWLEDGMENTS

The authors thank the following people from AbbVie: Li Li, Yuanyuan Sun, and Zheng Zhou for in vitro testing; Kent Stewart for helpful design and modeling discussions; Rodger Henry for the small-molecule X-ray structure of compound **17a**; Xiaoqin Liu for conscious telemetry mouse data with **17h**; Ron Pithawalla for expression and Anup Upadhyay for purification of PKCα protein for cocrystallization; and Russell Judge for growth of PKCα cocrystals with compound **28**. The X-ray crystal structure of PKCθ with compound **11a** was determined by Proteros Biostructures GmbH (Martinsried, Germany). Data for compound **28** bound to PKCα were collected at IMCA-CAT 17ID. Use of the IMCA-CAT beamline 17-ID (or 17-BM) at the Advanced Photon Source was supported by the companies of the Industrial Macromolecular Crystallography Association through a contract with Hauptman-Woodward Medical Research Institute. Use of the Advanced Photon Source was supported by the U.S. Department of Energy, Office of Science, Office of Basic Energy Sciences, under Contract DE-AC02-06CH11357.

■ ABBREVIATIONS USED

CV, cardiovascular; Con A, concanavalin A; CSA, cyclosporin A; GPI, glucose phosphate isomerase; IBD, inflammatory bowel disease; IL-2, interleukin-2; MDCK-MDR, Madin Darby canine kidney cells with the MDR gene; met ID, metabolite identification; PK, pharmacokinetics; PKC, protein kinase C; RA, rheumatoid arthritis; VDW, van der Waals

■ REFERENCES

(1) George, D. M.; Breinlinger, E. C.; Friedman, M.; Zhang, Y.; Wang, J.; Argiriadi, M.; Bansal-Pakala, P.; Barth, M.; Duignan, D. B.; Honore, P.; Lang, Q.; Mittelstadt, S.; Potin, D.; Rundell, L.; Edmunds, J. J. Discovery of selective and orally bioavailable protein kinase Cθ (PKCθ) inhibitors from a fragment hit. *J. Med. Chem.* **2014**, DOI: 10.1021/jm500669m.

(2) George, D. M.; Argiriadi, M. A.; Barth, M.; Bonafoux, D. F.; Breinlinger, E. C.; Dai, L.; Edmunds, J. J.; Friedman, M.; Guillier, F.; Hobson, A. D.; Potin, D.; Thomas, D.; Wang, J.; Wu, W.; Zhang, Y. Triazinone compounds. Patent WO2014089904, 2014.

(3) Altman, A.; Isakov, N.; Baier, G. Protein kinase Cθ: A new essential superstar on the T-cell stage. *Immunol. Today* **2000**, *21*, 567−573.

(4) Isakov, N.; Altman, A. Protein kinase Cθ in T cell activation. *Annu. Rev. Immunol.* **2002**, *20*, 761−794.

(5) Altman, A.; Villalba, M. Protein kinase Cθ (PKCθ): A key enzyme in T cell life and death. *J. Biochem.* **2002**, *132*, 841−846.

(6) Cywin, C. L.; Dahmann, G.; Prokopowicz, A. S., III; Young, E. R.; Magolda, R. L.; Cardozo, M. G.; Cogan, D. A.; DiSalvo, D.; Ginn, J. D.; Kashem, M. A.; Wolak, J. P.; Homon, C. A.; Farrell, T. M.; Grbic, H.; Hu, H.; Kaplita, P. V.; Liu, L. H.; Spero, D. M.; Jeanfavre, D. D.;

O'Shea, K. M.; White, D. M.; Woska, J. R., Jr.; Brown, M. L. Discovery of potent and selective PKC-θ inhibitors. *Bioorg. Med. Chem. Lett.* **2007**, *17*, 225−230.
(7) Roughten, A.; Rong, Y.; Ho, K.-K.; Ohlmeyer, M.; Diller, D. Purinones and 1*H*-imidazopyridinones as PKCθ inhibitors. Patent WO2008143674 A1, 2008.
(8) Roughton, A.; Ho, K.-K.; Ohlmeyer, M.; Diller, D.; Neagu, I.; Kingsbury, C.; Chan, J.-H.; Lommerse, M.; Teerhuis, M.; Wijkmans, M.; Plate, R. Pyrrolo[2,3-*d*]pyrimidin-2-yl-amine derivatives as PKCθ inhibitors and their preparation. Patent CA2716202 A1, 2009.
(9) Cole, D. C.; Asselin, M.; Brennan, A.; Czerwinski, R.; Ellingboe, J. W.; Fitz, L.; Greco, R.; Huang, X.; Joseph-McCarthy, D.; Kelly, M. F.; Kirisits, M.; Lee, J.; Li, Y.; Morgan, P.; Stock, J. R.; Tsao, D. H.; Wissner, A.; Yang, X.; Chaudhary, D. Identification, characterization and initial hit-to-lead optimization of a series of 4-arylamino-3-pyridinecarbonitrile as protein kinase C theta (PKCθ) inhibitors. *J. Med. Chem.* **2008**, *51*, 5958−5963.
(10) Prashad, A. S.; Wang, D.; Subrath, J.; Wu, B.; Lin, M.; Zhang, M. Y.; Kagan, N.; Lee, J.; Yang, X.; Brennan, A.; Chaudhary, D.; Xu, X.; Leung, L.; Wang, J.; Boschelli, D. H. C-5 substituted heteroaryl-3-pyridinecarbonitriles as PKCθ inhibitors: Part II. *Bioorg. Med. Chem. Lett.* **2009**, *19*, 5799−5802.
(11) Subrath, J.; Wang, D.; Wu, B.; Niu, C.; Boschelli, D. H.; Lee, J.; Yang, X.; Brennan, A.; Chaudhary, D. C-5 Substituted heteroaryl 3-pyridinecarbonitriles as PKCθ inhibitors: Part I. *Bioorg. Med. Chem. Lett.* **2009**, *19*, 5423−5425.
(12) Dushin, R. G.; Nittoli, T.; Ingalls, C.; Boschelli, D. H.; Cole, D. C.; Wissner, A.; Lee, J.; Yang, X.; Morgan, P.; Brennan, A.; Chaudhary, D. Synthesis and PKCθ inhibitory activity of a series of 4-indolylamino-5-phenyl-3-pyridinecarbonitriles. *Bioorg. Med. Chem. Lett.* **2009**, *19*, 2461−2463.
(13) Wu, B.; Boschelli, D. H.; Lee, J.; Yang, X.; Chaudhary, D. Second generation 4-(4-methyl-1*H*-indol-5-ylamino)-2-phenylthieno-[2,3-*b*]pyridine-5-carbonitrile PKCθ inhibitors. *Bioorg. Med. Chem. Lett.* **2009**, *19*, 766−769.
(14) Wagner, J.; von Matt, P.; Sedrani, R.; Albert, R.; Cooke, N.; Ehrhardt, C.; Geiser, M.; Rummel, G.; Stark, W.; Strauss, A.; Cowan-Jacob, S. W.; Beerli, C.; Weckbecker, G.; Evenou, J. P.; Zenke, G.; Cottens, S. Discovery of 3-(1*H*-indol-3-yl)-4-[2-(4-methylpiperazin-1-yl)quinazolin-4-yl]pyrrole-2,5-dione (AEB071), a potent and selective inhibitor of protein kinase C isotypes. *J. Med. Chem.* **2009**, *52*, 6193−6196.
(15) Wagner, J.; von Matt, P.; Faller, B.; Cooke, N. G.; Albert, R.; Sedrani, R.; Wiegand, H.; Jean, C.; Beerli, C.; Weckbecker, G.; Evenou, J. P.; Zenke, G.; Cottens, S. Structure−activity relationship and pharmacokinetic studies of sotrastaurin (AEB071), a promising novel medicine for prevention of graft rejection and treatment of psoriasis. *J. Med. Chem.* **2011**, *54*, 6028−6039.
(16) Jimenez, J. M.; Boyall, D.; Brenchley, G.; Collier, P. N.; Davis, C. J.; Fraysse, D.; Keily, S. B.; Henderson, J.; Miller, A.; Pierard, F.; Settimo, L.; Twin, H. C.; Bolton, C. M.; Curnock, A. P.; Chiu, P.; Tanner, A. J.; Young, S. Design and optimization of selective protein kinase C θ (PKCθ) inhibitors for the treatment of autoimmune diseases. *J. Med. Chem.* **2013**, *56*, 1799−1810.
(17) Jimenez, J. M.; Davis, C.; Boyall, D.; Fraysse, D.; Knegtel, R.; Settimo, L.; Young, S.; Bolton, C.; Chiu, P.; Curnock, A.; Rasmussen, R.; Tanner, A.; Ager, I. Structure-based optimization of amino-pyridines as PKCθ inhibitors. *Bioorg. Med. Chem. Lett.* **2012**, *22*, 4645−4649.
(18) Schubert, D.; Maier, B.; Morawietz, L.; Krenn, V.; Kamradt, T. Immunization with glucose-6-phosphate isomerase induces T cell-dependent peripheral polyarthritis in genetically unaltered mice. *J. Immunol.* **2004**, *172*, 4503−4509.
(19) Matsumoto, I.; Zhang, H.; Yasukochi, T.; Iwanami, K.; Tanaka, Y.; Inoue, A.; Goto, D.; Ito, S.; Tsutsumi, A.; Sumida, T. Therapeutic effects of antibodies to tumor necrosis factor-α, interleukin-6 and cytotoxic T-lymphocyte antigen 4 immunoglobulin in mice with glucose-6-phosphate isomerase induced arthritis. *Arthritis Res. Ther.* **2008**, *10*, R66.
(20) Hegen, M.; Keith, J. C., Jr.; Collins, M.; Nickerson-Nutter, C. L. Utility of animal models for identification of potential therapeutics for rheumatoid arthritis. *Ann. Rheum. Dis.* **2008**, *67*, 1505−1515.
(21) *Molecular Operating Environment (MOE)*, version 2013.08; Chemical Computing Group: Montreal, QC, 2014.